KeA1

CHINESE ROOTS
GLOBAL IMPACT

#### Contents lists available at ScienceDirect

## Petroleum Science

journal homepage: www.keaipublishing.com/en/journals/petroleum-science



## **Original Paper**

## Gas generation from oil-prone mudstones in the Eocene Wenchang A Depression, Pearl River Mouth Basin



Shu-Xia Li <sup>a</sup>, Bin Xu <sup>b</sup>, Shu-Qian Li <sup>a</sup>, Feng-Hua Zhao <sup>a,b</sup>, You-Chuan Li <sup>c</sup>, Hong-Fu Sun <sup>a</sup>, Le Lu <sup>d</sup>, Jin-Zhong Liu <sup>e,\*</sup>

- <sup>a</sup> College of Geoscience and Surveying Engineering, China University of Mining and Technology, Beijing, 100083, China
- <sup>b</sup> School of Safety Engineering, North China Institude of Science and Technology, Tangshan, 065201, Hebei, China
- <sup>c</sup> CNOOC Research Institute Co. Lid., Beijing, 100028, China
- <sup>d</sup> Power Environmental and Energy Research Institute, Covina, 91722, USA
- <sup>e</sup> State Key Laboratory of Deep Earth Processes and Resources, Guangzhou Institute of Geochemistry, Chinese Academy of Sciences, Guangzhou, 510640, Guangdong, China

#### ARTICLE INFO

#### Article history: Received 19 July 2024 Received in revised form 26 March 2025 Accepted 21 May 2025 Available online 27 May 2025

Edited by Xi Zhang

Keywords:
Oil-prone mudstones
Wenchang Formation
Primary cracking
Secondary cracking
Gaseous hydrocarbons generation process

#### ABSTRACT

Gas derived from the primary cracking of kerogen and the secondary cracking of oil has historically been the focus of petroleum geologists, given its importance as a gas source. The Wenchang A Depression within the Zhu III Sub-basin is the largest gaseous hydrocarbon-rich depression in the Pearl River Mouth Basin (PRMB), and the sources of gaseous hydrocarbons in this depression are a research focus. Mudstones from the Eocene Wenchang Formation contain type I and type II organic matter and are oilprone, with TOC, S1+S2, and HI values mostly ranging from 1.42% to 3.12%, 9.71 mg/g to 20.61 mg/g, and 410.71 mg/g TOC to 736.17 mg/g TOC, respectively. Data of gaseous hydrocarbon yields and carbon isotopic compositions show that the gaseous hydrocarbons generated from oil-prone mudstones are mainly derived from the secondary cracking of oil, and the plot of  $\delta^{13}C_2 - \delta^{13}C_3$  versus  $\ln(C_2/C_3)$  effectively identified the gas source. To further assess the gas generation processes and the ratio of oil-cracking gas under geological conditions, we reconstructed the history of gaseous hydrocarbon generation in mudstones from the Wenchang Formation in the Wenchang A Depression. Results showed that gaseous hydrocarbon generation began at approximately 33 Ma, a maximum of 69% of total gaseous hydrocarbons ( $C_1$ – $C_5$ ) was generated by oil cracking, and total heavy hydrocarbon gases ( $C_2$ - $C_5$ ) were mainly generated from oil cracking (65%-81%). This study provides a deeper understanding of the characteristics of gas generated from oil-prone mudstones and is important for gas exploration in the Wenchang Depression.

© 2025 The Authors. Publishing services by Elsevier B.V. on behalf of KeAi Communications Co. Ltd. This is an open access article under the CC BY-NC-ND license (http://creativecommons.org/licenses/by-nc-nd/4.0/).

## 1. Introduction

Natural gas can be produced in two ways under geological conditions: primary cracking of kerogen and secondary cracking of oil (Berner et al., 1995; Tang et al., 2000; Tian et al., 2012; Wang et al., 2017). Primary cracking of kerogen relates to the direct formation of gases from the thermal cracking of kerogen, while secondary cracking of oil relates to the gases produced from the

E-mail address: liujinz@gig.ac.cn (J.-Z. Liu).

Peer review under the responsibility of China University of Petroleum (Beijing).

cracking of oil caused by the primary cracking of kerogen (Behar et al., 1992; Prinzhofer and Huc, 1995). Kerogen and oil cracking gases are the comprehensive result of chemical, physical and geological processes. Identifying gases derived from primary or secondary cracking and quantifying their proportions are currently important issues in evaluating and exploring natural gas resources (Hu et al., 2005; Tian et al., 2010; Guo et al., 2009; Wang et al., 2018). Studies have primarily used isotope data and the composition of natural gas obtained from the field and in the laboratory to distinguish between oil-cracking and kerogen-cracking gases (Prinzhofer and Huc, 1995; Lorant et al., 1998; Cramer, 2004; Tian et al., 2012; Zhang et al., 2018). However, directly applying experimental results to geological conditions does not produce

 $<sup>\</sup>ast$  Corresponding author.

accurate reconstructions of geological processes, and kinetic methods based on pyrolysis experiments have become an important means of studying gas generation and are widely used in global research (Dieckmann et al., 1998; Hill et al., 2003; Peters et al., 2018).

The Zhu III Sub-basin is an important petroleum-bearing basin in the Pearl River Mouth Basin (PRMB) (Yang et al., 2019: He et al., 2024). This sub-basin contains two sets of source rocks, the Wenchang and Enping Formations; of these, the Wenchang Formation has a greater oil generation potential than the latter (Huang et al., 2007; You et al., 2024). The Wenchang A Depression is the largest hydrocarbon-rich depression in the Zhu III Sub-basin and is mainly composed of natural gas, with natural gas resources of approximately  $1323 \times 10^8$  m<sup>3</sup> (Gao et al., 2024). The genesis, sources and generation histories of natural gases in the depression are popular research topics (Zhang et al., 2014; Wang et al., 2016; Quan et al., 2019). However, the results of studying natural gas sources and genesis in the Wenchang A Depression are inconsistent. For example, studies have shown that natural gas may be generated from the source rocks in the Enping Formation (Ji and Wang, 2004; Zhang et al., 2014; Wang et al., 2020), or from the source rocks of both the Enping Formation and Wenchang Formation (Gan, 2007; Huang et al., 2007) or from the source rocks of the Enping Formation and also from crude oil cracking and kerogen cracking gas from the Wenchang Formation (Wang et al., 2014; Quan et al., 2019).

The Wenchang Formation in the Wenchang A Depression has a deep burial depth, ranging from 5000 m to 9000 m (Wang et al., 2020), and wells have not been drilled into (Xiao et al., 2009: Cheng et al., 2015). Therefore, studies have systematically investigated the organic geochemical characteristics of the source rocks and the gas generation properties of the Enping Formation (Gan et al., 2012; Li et al., 2020; Liu et al., 2022), whereas few studies have investigated these aspects of the source rocks of the Wenchang Formation. Therefore, we selected source rock samples from the Wenchang Formation and used organic geochemical and experimental pyrolysis data and kinetic modelling to analyse its hydrocarbon generation potential and mechanism. The results revealed the variation patterns in carbon isotopes and the yield from kerogen cracking and oil cracking gases. The process of gaseous hydrocarbon generation from the source rocks of the Wenchang Formation in the Wenchang A Depression was then reconstructed.

## 2. Geological setting

The Zhu III Sub-basin is a continental margin fault basin located west of the Pearl River Mouth Basin (PRMB) (Fig. 1(a)). It covers approximately 3600 km<sup>2</sup> from a longitude of 124°30′ to 127°00′ and latitude of 19°00′ to 31°59′ (Fu et al., 2011). Structurally, the Zhu III Sub-basin can be subdivided into 11 subunits: the Wenchang A, B, C, D, and E depressions; the Qionghai Depression; the Yangjiang Depression; the Yangchun Uplift; the Yangjiang Uplift; the Qionghai Uplift and the Shenhu Uplift (Quan et al., 2017, Fig. 1 (b)). Currently, oil and gas exploration in sub-basins is mainly concentrated in the Wenchang A and B Depressions; oil is primarily generated in the Wenchang B Depression, whereas gas is primarily generated in the Wenchang A Depression (Huang et al., 2003; Gan et al., 2009; Quan et al., 2017). The Wenchang A and B depressions are situated in the central part of the Zhu III Sub-basin, which exhibits a general NE-SW trend (Fig. 1(b)). The tectonic evolution of the Zhu III Sub-basin is subdivided into two stages: a syn-rifting stage from the Palaeocene to the early Oligocene, and a later subsiding stage from the late Oligocene to the present (Gong and Li, 2004; Cai, 2005).

The Cenozoic strata in the Zhu III Depression have a maximum thickness of 10000 m and include nine formations: Shehu, Wenchang, Enping, Zhuhai, Zhujiang, Haijiang, Yuehai, Wanshan and Qionghai (Jiang et al., 2009) (Fig. 2). The main effective source rocks are distributed in the Eocene Wenchang and Oligocene Enping formations, with the main reservoirs in the Oligocene Zhuhai and Miocene Zhujiang formations and the main seals in the Miocene Haijiang and Yuehai formations (Zhu et al., 1999; Gong and Li, 2004; Cheng et al., 2013).

This study focuses on the Eocene Wenchang Formation, which was deposited in a lacustrine sedimentary environment (Jiang et al., 2009; Li et al., 2020). The formation primarily comprises sandstone and mudstone, which have a cumulative thickness of 800-1500~m

## 3. Material and methods

## 3.1. Samples

It is not possible to obtain samples from the Wenchang Formation in the Wenchang A Depression due to the reasons discussed in the Introduction section. However, the Wenchang A and B depressions are adjacent and have undergone the same geological evolutionary process with minimal variations in source rock characteristics between the two depressions (Gong and Li, 2004; Cheng et al., 2015; Zhou et al., 2018). Therefore, samples from the Wenchang B Depression were selected, as these are representative of the Wenchang A Depression. Ten mudstone samples were obtained from the Wenchang B Depression, including one sample from Well L-1, four samples from Well L-2 and five samples from Well L-3 (Table 1). The specific locations of the wells are shown in Fig. 1.

All the selected samples were ground to 200 mesh for organic geochemical analysis. In addition, a 200-mesh mudstone sample (A-1) was selected for confined pyrolysis experiments. The mudstone samples required further preparations. First, HF and HCL treatments were applied to remove inorganic minerals from the mudstone and produce initial kerogen (named I-kerogen). Ikerogen was then divided into two parts: the first part was directly used in a confined pyrolysis experiment to reproduce the entire gas generation process from the total organic matter, and both kerogen- and oil-cracking gases were obtained. The other part (1012.01 mg) was kept at 350 °C for 72 h in a glass tube to obtain extracted oil (320.90 mg) and de-oiled kerogen (683.06 mg) (Fig. 3). In this respect, the oil was extracted using a Soxhlet extractor with a methanol: acetone: benzene mixture (MAB: 1:2.5:2.5 v:v:v) over 72 h. The extracted oil was composed of two parts: oil expelled from kerogen collected by the cold trap, and oil retained in the heated kerogen. The extracted oil (named E-oil) and de-oiled kerogen (named D-kerogen) were used to study trends in the evolution and amount of oil cracking gas and kerogen cracking gas, respectively. This simple experimental procedure is illustrated in Fig. 4.

#### 3.2. Organic geochemistry analysis

Total organic carbon (TOC), Rock-Eval pyrolysis, and vitrinite reflectance ( $R_0$ ) organic geochemical analyses were performed using a LECO C230, an OGE-II instrument and a Leica DMRX microscope, respectively, at the Guangzhou Institute of Geochemistry, Chinese Academy of Sciences, and the procedures followed were based on the GB/T19145–2003, GB/T18602-2001 and GBT6948-2008 guidelines, respectively. The Rock-Eval pyrolysis data included free hydrocarbons (S1), pyrolysis hydrocarbons (S2)

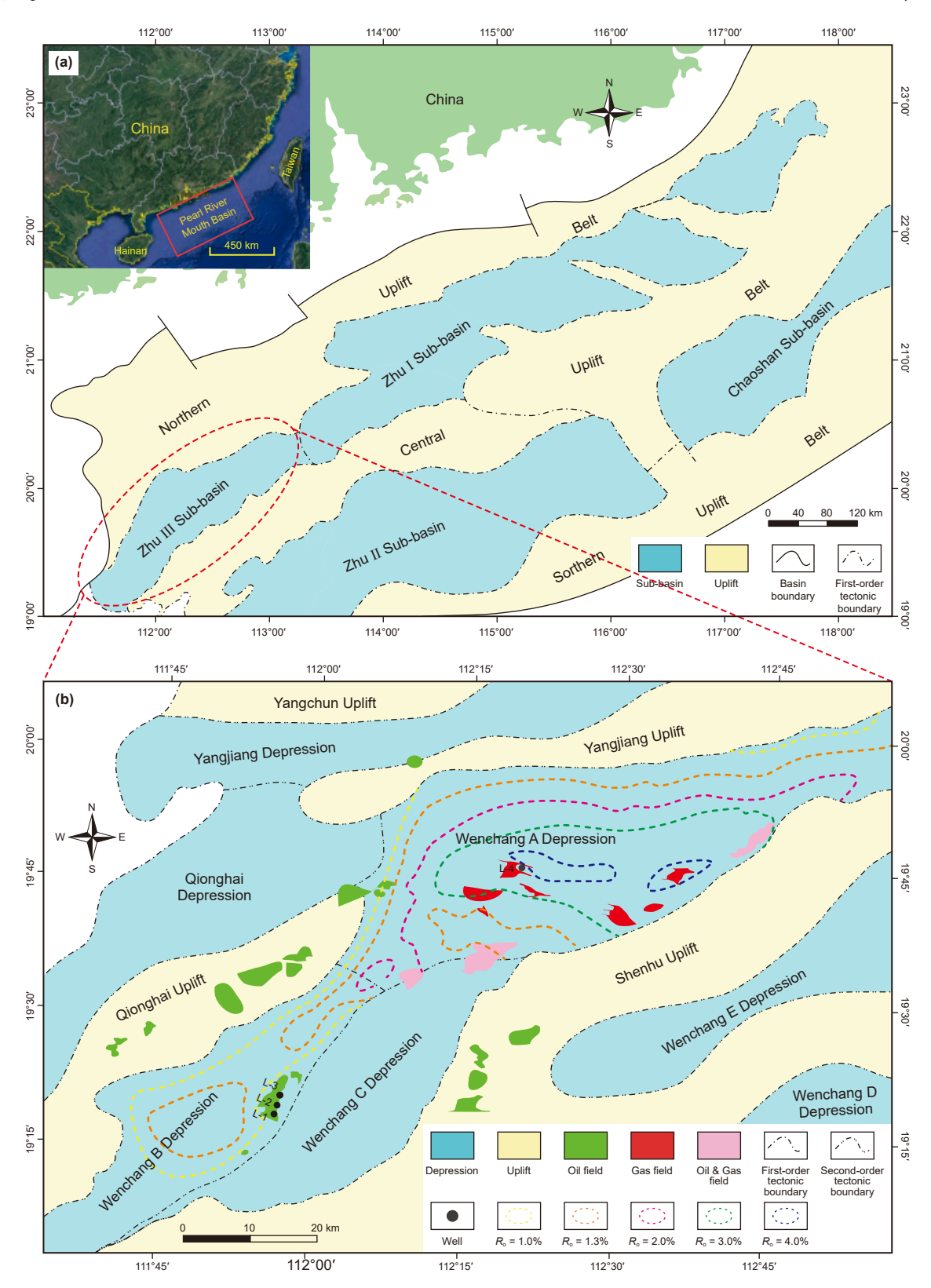


Fig. 1. Map showing the structural elements of the Pearl River Mouth Basin (a) and geological structure of the Zhu III Sub-basin (b) (modified from Quan et al., 2017; Wang et al., 2020).

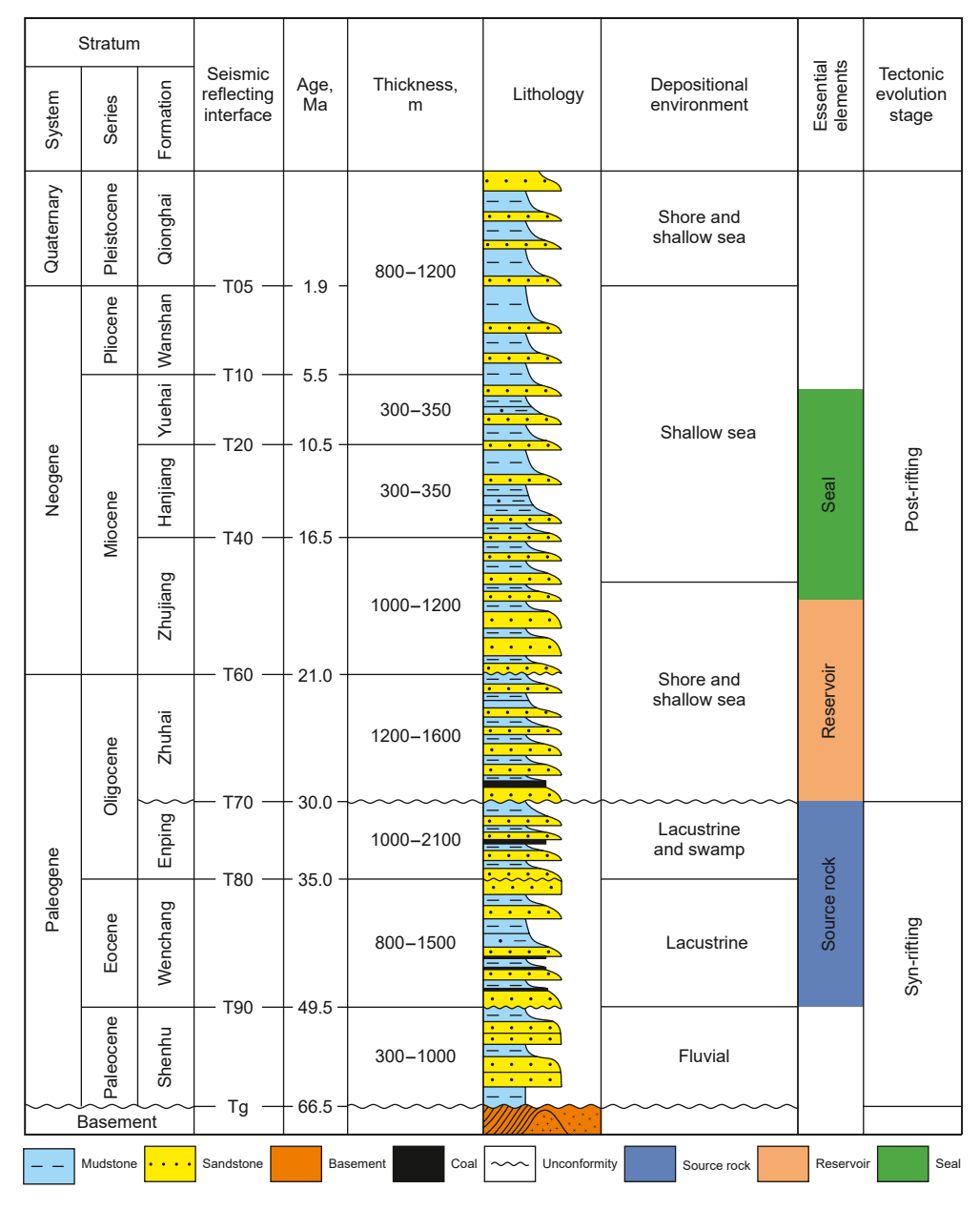


Fig. 2. Columnar section showing the stratigraphy, tectonics and petroleum geology of the Cenozoic in the Zhu III Sub-basin (modified from Gong and Li, 2004; Jiang et al., 2009).

**Table 1**Organic geochemistry data of mudstones.

Well	Sample name	R <sub>0</sub> , %	TOC, %	S1, mg/g	S2, mg/g	S1+S2, mg/g	T <sub>max</sub> , °C	HI, mg/g·TOC
L-1	A-1	0.72	3.12	0.18	19.78	19.96	434	633.97
	I-kerogen	0.72	53.70	1.95	340.13	342.08	434	633.39
	D-kerogen	1.08	49.56	0.12	121.79	121.91	467	245.98
	E-oil	1	75.87	1	1	1	1	1
L-2	A-2	1	1.42	0.31	8.20	8.51	443	578.72
	A-3	1	1.84	0.84	8.87	9.71	442	480.85
	A-4	1	1.90	0.66	10.91	11.57	443	574.47
	A-5	1	2.57	1.72	18.90	20.61	443	736.17
L-3	A-6	1	0.57	0.15	2.33	2.49	443	410.71
	A-7	1	1.89	1.17	11.61	12.78	446	613.10
	A-8	Ì	2.46	1.15	12.16	13.31	445	494.05
	A-9	1	2.67	1.31	14.49	15.80	449	541.67
	A-10	1	3.20	3.31	16.93	20.24	453	529.76

and the temperature corresponding to the peak value of hydrocarbon generation ( $T_{\text{max}}$ ).

## 3.3. Confined pyrolysis experiments

The confined and anhydrous pyrolysis experiments were conducted at the Guangzhou Institute of Geochemistry, Chinese Academy of Sciences. The I-kerogen, D-kerogen and E-oil samples were divided into 34, 24 and 24 aliquots, respectively. These were sealed into gold tubes (5.5 mm outer diameter, 0.25 mm wall thickness, and 60 mm length) in an argon atmosphere and then placed into stainless-steel pressure vessels. Pyrolysis was performed at a constant confining pressure of 50 MPa with a permitted error of less than 1 MPa. The vessels were heated in an oven from 20 °C to 200 °C over 10 h, and then from 200 °C to 600 °C at a rate of 2 °C/h and 20 °C/h. Following pyrolysis, the gold tubes were taken out, cooled, placed in a vacuum container and then pierced to release the gas, which was directly injected into a gas chromatograph (GC5890) to conduct a quantitative analysis of the methane  $(C_1)$ , ethane  $(C_2)$ , propane  $(C_3)$ , butane  $(C_4)$  and pentane  $(C_5)$  components. When analysing variations in the gaseous hydrocarbon yields, the sum of the individual heavy hydrocarbon gases was defined as the total heavy hydrocarbon gases  $(C_2-C_5)$ , and the sum of  $C_1$  and  $C_2-C_5$  was defined as the total gaseous hydrocarbon ( $C_1$ – $C_5$ ). In addition, owing to the low  $C_4$  and  $C_5$  yields, the pattern of variation in the sum of these two products  $(C_4-C_5)$  was analysed.

The carbon isotopic composition of the gaseous hydrocarbons was ascertained using a Delta Plus XL gas chromatography-isotope ratio mass spectrometer (GC-IRMS). For the GC, we employed a Poraplot Q capillary column (30 m  $\times$  0.32 mm  $\times$  0.25  $\mu m)$  and helium carrier gas. The samples were placed in a GC oven, maintained at 40 °C for 5 min, heated to 190 °C at a rate of 15 °C/min, and then held for 15 min at 190 °C. The obtained isotopic data included methane carbon isotope ( $\delta^{13}C_1$ ), ethane carbon isotope ( $\delta^{13}C_2$ ) and propane carbon isotope ( $\delta^{13}C_3$ ) data.

## 3.4. Burial and geothermal history reconstruction

The first step in studying the hydrocarbon generation process of a region involves examining and reconstructing the burial and thermal evolution processes (Hakimi et al., 2010; Liu et al., 2015; Liu et al., 2022). Detailed geological parameters of the Wenchang A Depression were obtained from the China National Offshore Oil Co Research Institute Co. Ltd.

We used PetroMod (1D) modelling software to reconstruct the burial and geothermal history of Well L-4 in the Wenchang A Depression of the Zhu III Sub-basin within the PRMB (the specific location is shown in Fig. 1). The detailed geological parameters of the well, including the formation thickness, burial depth, rock

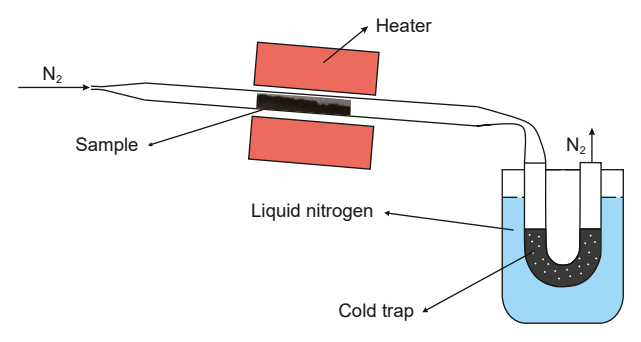


Fig. 3. Diagram of simple device used to obtain D-kerogen and E-oil samples.

density, initial porosity, compaction factor, lithological composition,  $R_0$  and bottom hole temperature (BHT) were obtained from the China National Offshore Oil Co Research Institute Co. Ltd.

#### 4. Results

#### 4.1. Organic geochemical data

Organic geochemical data from the mudstones of the Wenchang Formation are presented in Table 1. The TOC, S1 and S2 ranged from 0.57% to 3.20%, 0.12 mg/g to 3.31 mg/g and 2.33 mg/g to 19.78 mg/g, respectively. The hydrogen index (HI =  $100 \times S2/TOC$ ) was used to evaluate the hydrocarbon potential of the source rocks (Espitalié et al., 1985), and the HI values of the mudstones ranged from 410.71 to 736.17 mg/g-TOC.

Mudstone sample A-1, which was selected for the confined pyrolysis experiment, had a relatively low Ro value of 0.72% with TOC, S1, S2 and HI values of 3.12%, 0.18 mg/g, 19.78 mg/g and 633.97 mg/g·TOC, respectively. For I-kerogen, the Ro value remained unchanged at 0.72%, and the TOC, S1, S2 and HI values were 53.70%, 1.95 mg/g, 340.13 mg/g and 633.39 mg/g·TOC, respectively. For D-kerogen, the measured  $R_0$  value, TOC, S1, S2 and HI values were 1.08%, 49.56%, 0.12 mg/g, 121.79 mg/g and 245.98 mg/g·TOC, respectively.

## 4.2. Gaseous hydrocarbon yields

Trends in variations of the methane (C<sub>1</sub>) yield generated were the same for I-kerogen, D-kerogen and E-oil (Table 2, Fig. 5(a) and (b)), and the methane yield gradually increased with increasing temperature during the pyrolysis experiments. Taking the experimental run of 2 °C/h as an example, the C<sub>1</sub> yields of I-kerogen, E-oil and D-kerogen were 1.28 mL/g·I-kerogen, 0.07 mL/g·I-kerogen and 0.59 mL/g·I-kerogen, respectively, at the set initial temperature. The yields then gradually increased with the increasing temperatures, reaching 287.10 mL/g·I-kerogen, 48.46 mL/g·I-kerogen, 192.32 mL/g·I-kerogen at 600 °C, respectively.

There were differences between the trends in methane and heavy gaseous hydrocarbons ( $C_2$ ,  $C_3$  and  $C_4$ – $C_5$ ) from I-kerogen, D-kerogen and E-oil (Table 2; Fig. 5 (c), (d), (e), (f), (g) and (h)). The yields of  $C_2$ ,  $C_3$  and  $C_4$ – $C_5$  increased with increasing pyrolysis temperature until they reached their maximum values, and then decreased in relation to cracking effects. Notably, the yield of heavy hydrocarbon gases varied with the number of carbon atoms. The higher the number of carbon atoms in the heavy hydrocarbon gas, the lower the temperature corresponding to the maximum yield. Taking the yields of  $C_2$ ,  $C_3$  and  $C_4$ – $C_5$  generated by I-kerogen at 20 °C/h as an example, the maximum yields of  $C_2$ ,  $C_3$  and  $C_4$ – $C_5$  were 49.12 mL/g-I-kerogen at 551.0 °C, 21.59 mL/g-I-kerogen at 517.0 °C and 7.58 mL/g-I-kerogen at 500.3 °C, respectively.

For  $C_1$ – $C_5$ , the  $C_1$  yield accounted for the largest proportion, and the  $C_2$  yield accounted for the largest proportion of  $C_2$ – $C_5$ . Therefore, the variation trend in the  $C_1$ – $C_5$  yield was the same as that of  $C_1$  (Table 2, Fig. 5(k) and (l)), and the trend in the  $C_2$ – $C_5$  yield was similar to that of  $C_2$  (Table 2, Fig. 5(i) and (j)).

## 4.3. Kinetic parameters of gaseous hydrocarbon

A set of parallel first-order reactions with a single frequency factor (A) and activation energy (E) distribution are used to describe the petroleum generated by kerogens (Espitalié et al., 1988; Behar et al., 1997). The frequency factor is the total number of effective collision frequencies of the activated molecules, and the activation energy is the minimum energy required for a chemical reaction. The frequency factor is correlated with the

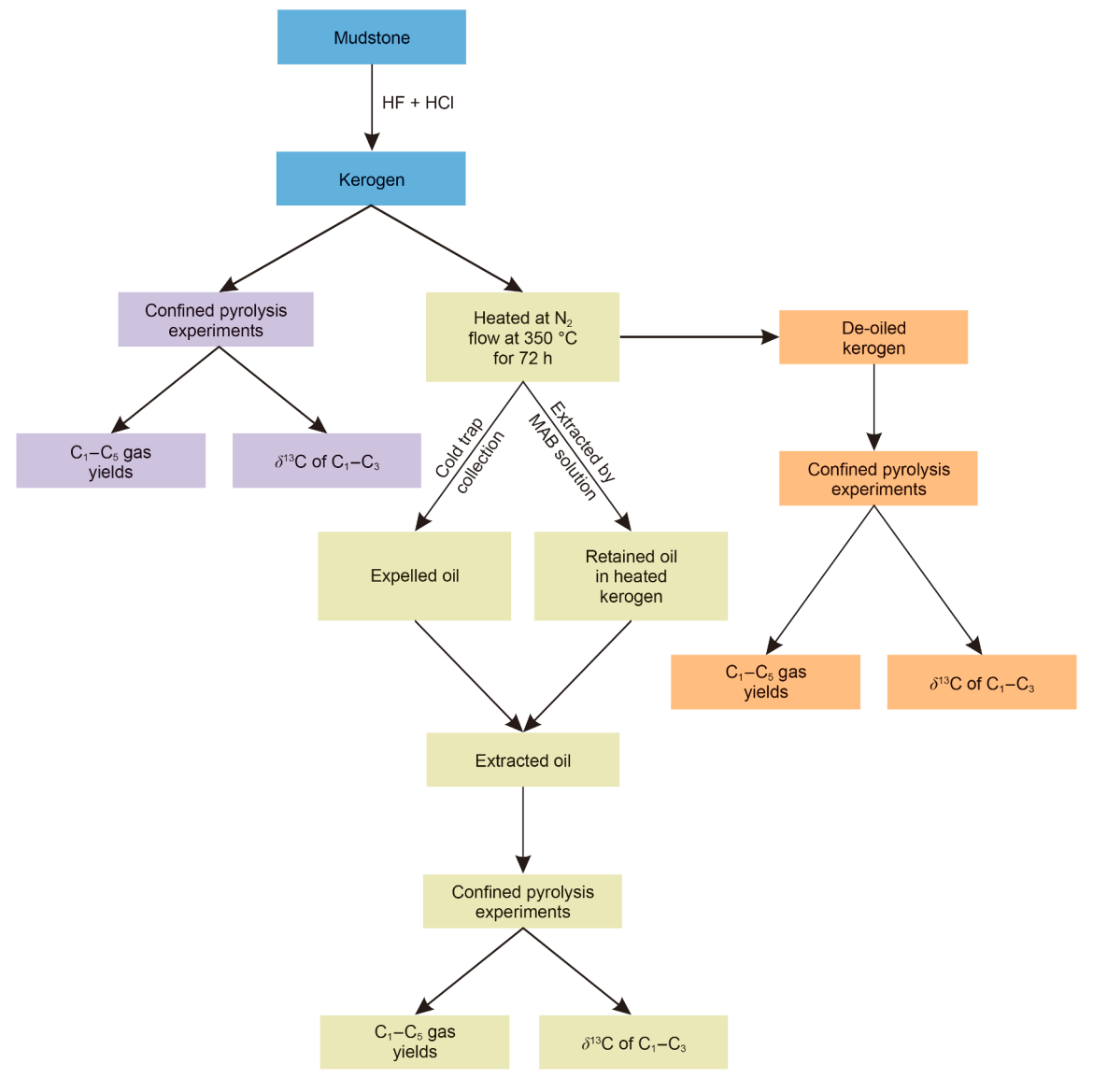


Fig. 4. Flowchart of confined pyrolysis experimental procedure and associated products.

hydrocarbon generation activation energy (Pelet, 1994; Waples, 2000; Pan et al., 2012). The higher the activation energy, the greater the energy required for conversion and the higher the temperature required for the reaction, and the faster the particle moves, the higher the frequency factor. In this study, the discrete model in KINETICS 2000 software (Burnham and Braun, 1999) was used to calculate the kinetic parameters of hydrocarbon generation. When calculating kinetic parameters of hydrocarbon generation, it is necessary to determine the maximum hydrocarbon vield of the sample (Liu and Tang, 1998). However, due to the incomplete pyrolysis experiments conducted in this study, the maximum yield of each gaseous hydrocarbon was not obtained. Therefore, maximum values for different gaseous hydrocarbons were iteratively assumed and used as input into the KINETICS 2000 software to calculate the total error between the experimental data points and the theoretical curve. The maximum hydrocarbon yield values were then determined when the error was minimal. The assumed maximum values of  $C_1$ ,  $C_2$ – $C_5$  and  $C_1$ – $C_5$  generated by I-kerogen, D-kerogen and E-oil are shown in Table 3. The kinetic

parameters and fitting curves for  $C_1$ ,  $C_2$ – $C_5$  and  $C_1$ – $C_5$  generated by I-kerogen, D-kerogen and E-oil are shown in Table 3 and Figs. 6–8.

The characteristics of the variations in the kinetic parameters  $C_1$ ,  $C_2$ – $C_5$  and  $C_1$ – $C_5$  for I-kerogen, D-kerogen and E-oil differed. The frequency factor and activation energies of the gaseous hydrocarbons from E-oil were the largest, followed by those from I-kerogen, whereas those of D-kerogen were the smallest. Taking the kinetic parameters of  $C_1$  as an example, the frequency factor from E-oil was the largest  $(1.11 \times 10^{14} \text{ s}^{-1})$ , that from I-kerogen had an intermediate value  $(2.21 \times 10^{12} \text{ s}^{-1})$  and that from D-kerogen was the smallest  $(1.49 \times 10^{11} \text{ s}^{-1})$ . The same was true for the variations in the activation energies of  $C_1$  for all three samples: the average activation energy (Ea) of E-oil was the largest (67.15 kcal/mol), that of I-kerogen was moderate (60.36 kcal/mol) and that of D-kerogen was the smallest (54.52 kcal/mol).

Through further inversion, we found that the fitting effect between the yields of  $C_1$ ,  $C_2$ – $C_5$  and  $C_1$ – $C_5$  calculated from the kinetic parameters and those measured from the confined pyrolysis experiments was excellent, indicating that the obtained kinetic

**Table 2** Measured cumulative yields of the C<sub>1</sub> C<sub>2</sub>, C<sub>3</sub>, C<sub>4</sub>–C<sub>5</sub>, C<sub>2</sub>–C<sub>5</sub> and C<sub>1</sub>–C<sub>5</sub> components generated by I-kerogen, D-kerogen and E-oil.

Heating rate	Sample	e No.		T		$C_1$ $C_2$			C <sub>3</sub>	$C_3$ $C_4-C_5$			· I <sub>2</sub>		CO <sub>2</sub>		$H_2S$	
				°C		mL/g	-I-keroį	gen										
20 °C/h	I-kerog	gen-1		341.8		0.9	96	0.	.21	1 0.14		0.08	0.06			27.11		0.08
	I-kerog	gen-2		361.1		1.0	07	0.	0.34 0.19		0.08		0.04		:	28.63		0.20
	I-kerog	-		373.0		2.8			.95	0.54		0.24				35.32		0.32
	I-kerog			388.8		4.3		1.77 1.00			0.47				36.07		0.35	
	I-kerog			405.4					.53	1.78		1.08		0.55		52.37		0.43
	I-kerogen-6			422.0			11.17		.08	2.92		1.76		0.78		44.18		0.54
	I-kerog			437.9		15.6			.27	4.23		2.33		1.05		46.93		0.81
	I-kerog			454.0		19.1			61	5.82		4.10		1.28		49.40		1.36
	I-kerogen-9			470.8		28.3		13.		8.97		4.39	1.50		65.58			2.31
	I-kerogen-10 I-kerogen-11			485.3 500.3		39.8 53.0		18. 26.		12.70 17.70		6.68 7.58		2.10 2.44		67.24 67.05		2.82 3.09
	I-kerog			517.0		78.9		37.		21.59		5.88		2.98		52.35		2.41
	I-kerog			533.9		116.3		48.		21.54		3.09		4.61		65.02		2.67
	I-kerog			551.0		155.1		49.		12.04		0.99		5.25		61.85		2.67
	I-kerog			567.3		188.6		46.		4.68		0.25		6.77		66.58		2.76
	I-kerog			583.5		227.3		43.		1.32		0.07		8.66		73.65		2.85
	I-kerog	-		599.9		246.1		26.		0.24		0.01	1	0.34		68.37		2.61
2 °C/h	I-kerogen-18			343.6		1.2			.29	0.48		0.18		0.37		29.14		0.10
	I-kerog			357.6		4.6	51	1.	.89	1.07		0.53		0.20		38.94		0.14
	I-kerog	gen-20		373.0		6.9	95		.20	1.74		0.86		0.38		44.52		0.18
	I-kerog	gen-21		389.8		14.2			.54	3.71		2.29		0.67		48.05		0.49
	I-kerogen-22			406.0		21.9			.63	5.64		3.79		0.87	48.05		0.59	
	I-kerogen-23			422.4					14.24 8.86			5.43		1.18	56.55		1.05	
	I-kerogen-24			438.6	40.35		20.		13.05		7.23	1.49		65.61		1.71		
	I-kerogen-25			454.7	54.97			28.		18.81		7.84		1.85	68.03		2.19	
	I-kerogen-26			471.1 487.0	78.08		39.		25.64 26.06		9.68	2.33		67.68 69.55			2.81	
	I-kerogen-27 I-kerogen-28			502.6	101.06 134.99		45. 52.		25.13		6.99 2.89 4.52 3.58		74.17			2.78 2.91		
	I-kerogen-29			519.2	170.44			49.		11.21		0.89	4.96		66.68			2.62
	I-kerogen-30			536.0		215.3		38.		1.18		0.05		6.36		70.00		2.49
	I-kerogen-31			551.8				27.		0.26		0.03	7.30			72.54		2.28
	I-kerogen-32			568.6		268.96		13.53		0.10		0.00		8.16		73.83		2.34
	I-kerogen-33			584.7		280.02			86	0.03		0.00	8.51			77.04		2.08
	I-kerogen-34			600.0		287.1			17	0.01		0.00		9.30		80.27		2.05
Heating rate	Sample No.	T	C <sub>1</sub>	$C_2$	C <sub>3</sub>	C <sub>4</sub> -C <sub>5</sub>	H <sub>2</sub>	CO <sub>2</sub>	H <sub>2</sub> S	Sample No.	T	C <sub>1</sub>	$C_2$	C <sub>3</sub>	C <sub>4</sub> -C <sub>5</sub>	H <sub>2</sub>	CO <sub>2</sub>	H <sub>2</sub> S
		°C	mL/g·I-	-keroge	n						°C	mL/g·I-l	kerogen					
20 °C/h	D-kerogen-1	334.4	0.04	0.00	0.00	0.00	0.00	0.63	0.01	E-oil-1	334.4	0.21	0.05	0.05	0.01	0.01	0.81	0.16
,	D-kerogen-2	358.0	0.04	0.01	0.00	0.00	0.00	0.85	0.07	E-oil-2	358.0	0.46	0.09	0.07	0.02	0.01	1.06	0.33
	D-kerogen-3	382.3	0.13	0.02	0.00	0.00	0.00	1.14	0.15	E-oil-3	382.3	0.79	0.21	0.15	0.06	0.02	1.02	0.44
	D-kerogen-4	405.7	0.70	0.16	0.02	0.00	0.00	2.02	0.32	E-oil-4	405.7	1.72	0.58	0.41	0.20	0.04	1.56	0.74
	D-kerogen-5	430.3	2.66	0.74	0.11	0.01	0.02	3.23	0.58	E-oil-5	430.3	4.09	1.58	1.22	0.77	0.12	1.98	0.91
	D-kerogen-6	454.3	6.14	1.38	0.27	0.03	0.13	3.96	1.04	E-oil-6	454.3	9.44	4.24	3.39	2.72	0.28	2.43	0.94
	D-kerogen-7	478.3	13.38	1.94	0.20	0.02	0.15	6.26	2.33	E-oil-7	478.3	20.29	10.84	8.64	6.79	0.62	2.91	1.02
	D-kerogen-8	503.2	21.51	1.76	0.13	0.01	0.36	7.20	2.73	E-oil-8	503.2	38.40	21.40	14.80	7.42	1.24	3.08	1.19
	D-kerogen-9	527.2	28.64	0.86	0.02	0.00	0.31	8.28	2.62	E-oil-9	527.2	64.57	35.82	19.16	4.31	1.72	4.21	1.03
	D-kerogen-10	551.1	34.66	0.40	0.01	0.00	0.64	8.96	3.21	E-oil-10	551.1	99.01	36.92	11.16	1.20	2.03	3.90	1.26
	D-kerogen-11	575.0		0.17	0.00	0.00	0.63	11.70		E-oil-11	575.0	134.04		2.50	0.19		4.03	
2 °C/b	D-kerogen-12	599.1	43.19	0.11	0.00	0.00	0.79	11.99	2.07	E-oil-12	599.1	162.10	19.28	0.49	0.03	4.12	4.67	0.82
2 °C/h	D-kerogen-13 D-kerogen-14	335.0 359.0	0.07 0.36	0.01 0.09	0.00 0.02	0.00	0.00 0.02	1.28 2.07	0.27 0.29	E-oil-13 E-oil-14	335.0 359.0	0.59 1.37	0.21 0.43	0.25 0.31	0.03 0.13	0.02 0.04	1.23 1.51	0.38 0.59
	D-kerogen-15	383.0	1.49	0.09	0.02	0.00	0.02	2.66	0.29	E-011-14 E-0il-15	383.0	3.15	1.16	0.31	0.13	0.04	1.92	0.59
	D-kerogen-16	407.1	5.01	1.21	0.08	0.01	0.04	4.31	0.38	E-oil-15	407.1	7.26	2.79	2.01	1.32	0.09	2.12	1.06
	D-kerogen-17	431.1	11.52	1.85	0.23	0.03	0.08	5.63	1.29	E-oil-10	431.1	16.48	7.14	5.64	4.62	0.16	3.10	0.99
	D-kerogen-18	455.2	20.62	1.97	0.14	0.02	0.15	7.92	2.27	E-oil-18	455.2	30.90	16.23	12.60	8.50	0.77	3.52	1.00
	D-kerogen-19	490.0	32.54	0.90	0.02	0.00	0.24	10.17	2.50	E-oil-19	479.4	54.72	27.94	16.31	5.33	1.00	3.35	1.18
		504.3	36.63	0.47	0.00	0.00	0.46	10.31	2.42	E-oil-20	504.3	87.47	35.64	13.55	1.54	1.43	3.77	1.05
	D-kerogen-20							9.86	2.42	E-oil-21	528.0	123.26	33.49	4.02	0.34	1.89	4.89	1.02
	D-kerogen-20 D-kerogen-21	528.0	40.63	0.12	0.00	0.00	0.44	5.00	2.72		320.0					1.05		
			40.63 45.17	0.12 0.02	0.00	0.00	0.70	11.65	2.33	E-oil-22	552.1	161.43	21.26	0.55	0.05	2.40	4.29	0.92
	D-kerogen-21	528.0																

parameters were reliable and could be effectively used to simulate the hydrocarbon generation process under geological conditions (Peters et al., 2018).

## 4.4. Carbon isotope compositions

The carbon isotope values of  $C_1$ ,  $C_2$  and  $C_3$  from the I-kerogen, D-kerogen and E-oil exhibited the same trend with increasing

pyrolysis temperature (Fig. 9 and Table 4). With an increase in the thermal evolution,  $C_1$ ,  $C_2$  and  $C_3$  were gradually enriched in  $\delta^{12}C$ . They also reached their respective minimum  $\delta^{13}C$  values prior to becoming gradually enriched in  $\delta^{13}C$ , and their respective  $\delta^{13}C$  values then began to increase, as described by Hill et al. (2003). Taking the  $C_1$ ,  $C_2$  and  $C_3$  carbon isotope values at 20 °C/h from I-kerogen as examples, the minimum  $\delta^{13}C_1$ ,  $\delta^{13}C_2$  and  $\delta^{13}C_3$  values were reached at 454.0 °C, 470.8 °C and 454.0 °C, respectively, and

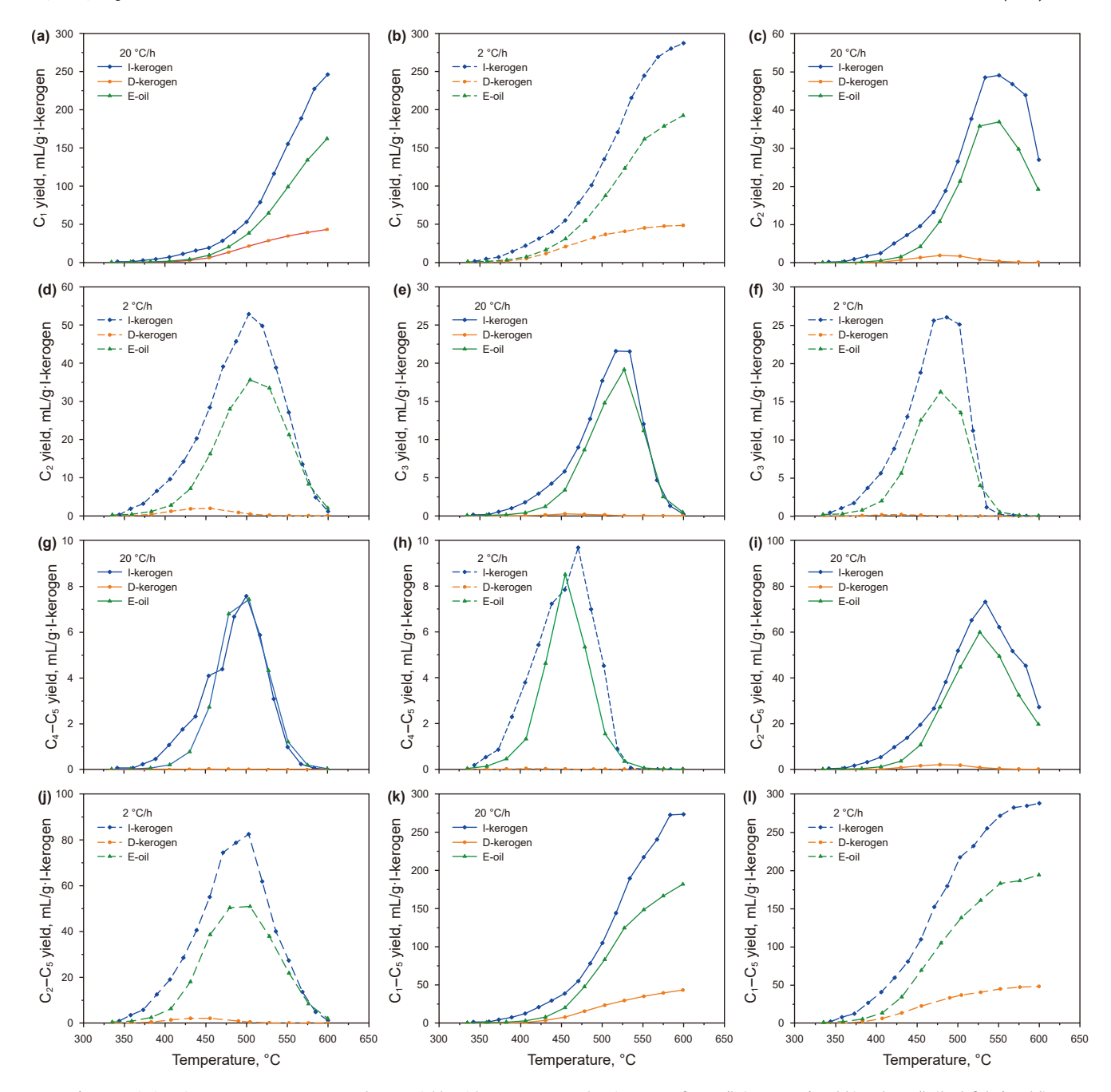


Fig. 5. Variations in  $C_1$   $C_2$ ,  $C_3$ ,  $C_4$ – $C_5$ ,  $C_2$ – $C_5$  and  $C_1$ – $C_5$  yields with temperature at heating rates of 20 °C/h (a, c, e, g, i and k) and 2 °C/h (b, d, f, h, j and l).

**Table 3**Kinetic parameters of gaseous hydrocarbons from I-kerogen, D-kerogen and E-oil.

Name	Max, mL/g·I-kerogen	Er, kcal·mol <sup>-1</sup>	Ea, kcal·mol <sup>-1</sup>	A, s <sup>-1</sup>
C <sub>1</sub> (I-kerogen)	290	48–66	60.36	2.21 × 10 <sup>12</sup>
C <sub>1</sub> (D-kerogen)	50	47–65	54.52	$1.49 \times 10^{11}$
C <sub>1</sub> (E-oil)	200	54–73	67.15	$1.11 \times 10^{14}$
C <sub>2</sub> -C <sub>5</sub> (I-kerogen)	86	42–60	52.31	2.11 × 10 <sup>11</sup>
C <sub>2</sub> -C <sub>5</sub> (D-kerogen)	2.5	48–52	48.77	$1.07 \times 10^{11}$
C <sub>2</sub> -C <sub>5</sub> (E-oil)	62	50–68	61.69	$1.21\times10^{14}$
C <sub>1</sub> -C <sub>5</sub> (I-kerogen)	295	44–64	55.68	3.90 × 10 <sup>11</sup>
C <sub>1</sub> -C <sub>5</sub> (D-kerogen)	51	47–64	54.06	$1.15 \times 10^{11}$
$C_1$ - $C_5$ (E-oil)	205	50–74	64.71	$1.00\times10^{14}$

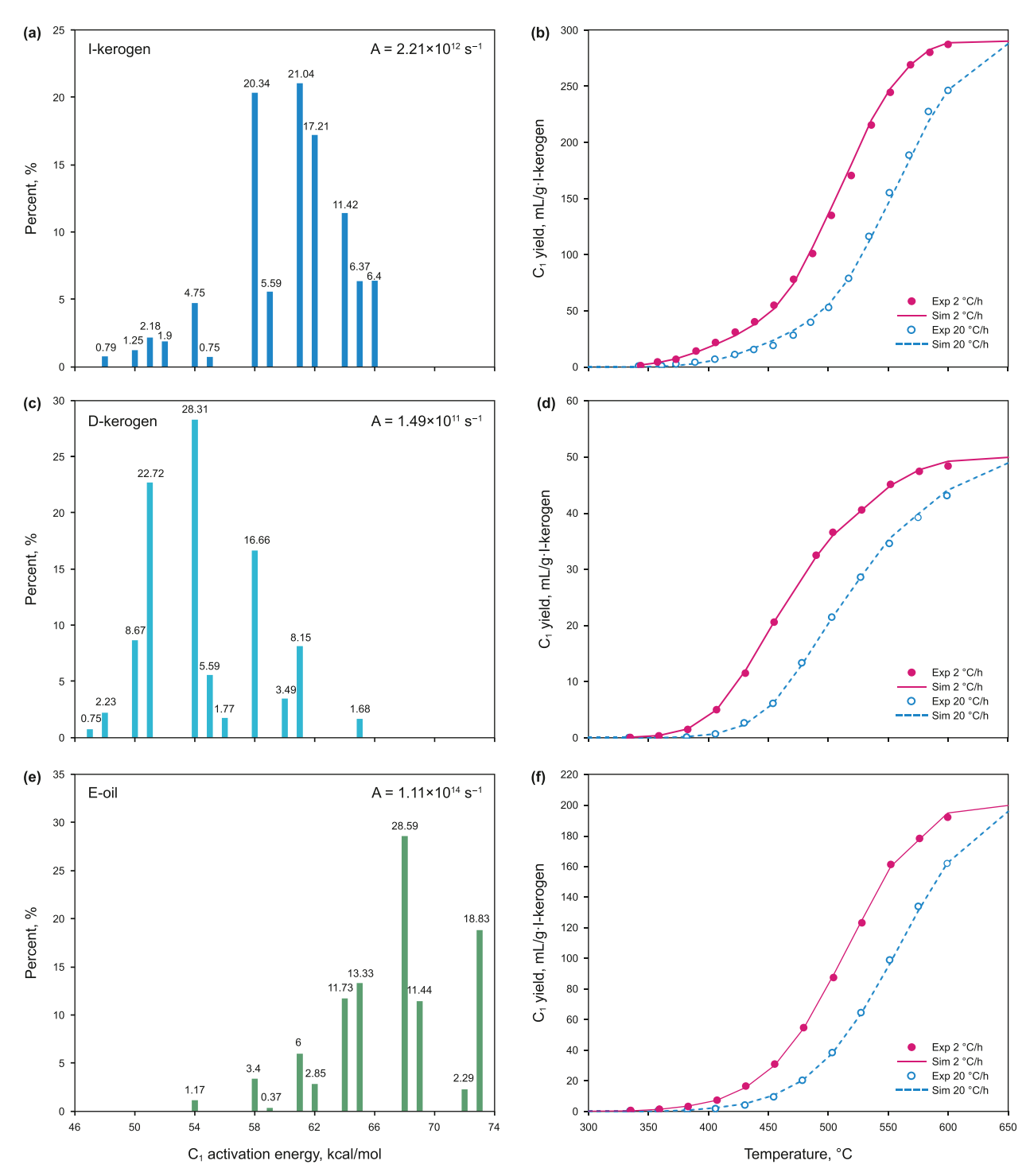


Fig. 6. Kinetic parameter distributions of C<sub>1</sub> (a, c and e) and fitting curves between the calculated (Sim) and measured (Exp) values of the C<sub>1</sub> yield (b, d and f) from I-kerogen, D-kerogen and E-oil.

they then began to gradually increase. This phenomenon is primarily attributed to the maturity of thermal evolution, the activation energy difference in chemical bond breakage, and the isotopic fractionation effect (Tang and Jenden, 1998; Tang et al., 2000; He et al., 2018). In the early pyrolysis stage, the  $\beta$ -fracture of long-chain alkyl molecules and the decomposition of nonhydrocarbons (NSO) are the main processes, leading to the preferential release of lighter carbon isotopes and a gradual decrease in  $\delta^{13}$ C values. At the same time, the activation energy of the

reaction is low, and the isotopic fractionation effect is small, resulting in a potentially lighter isotopic composition of the generated products. In the later pyrolysis stage, the cracking of short-chain alkyl molecules becomes the primary process, leading to a preference for heavier carbon isotopes to remain in the products, resulting in a gradual increase in  $\delta^{13}$ C values. Additionally, the high activation energy in the reaction and the significant isotopic fractionation effect may also contribute to the gradual increase in  $\delta^{13}$ C values.

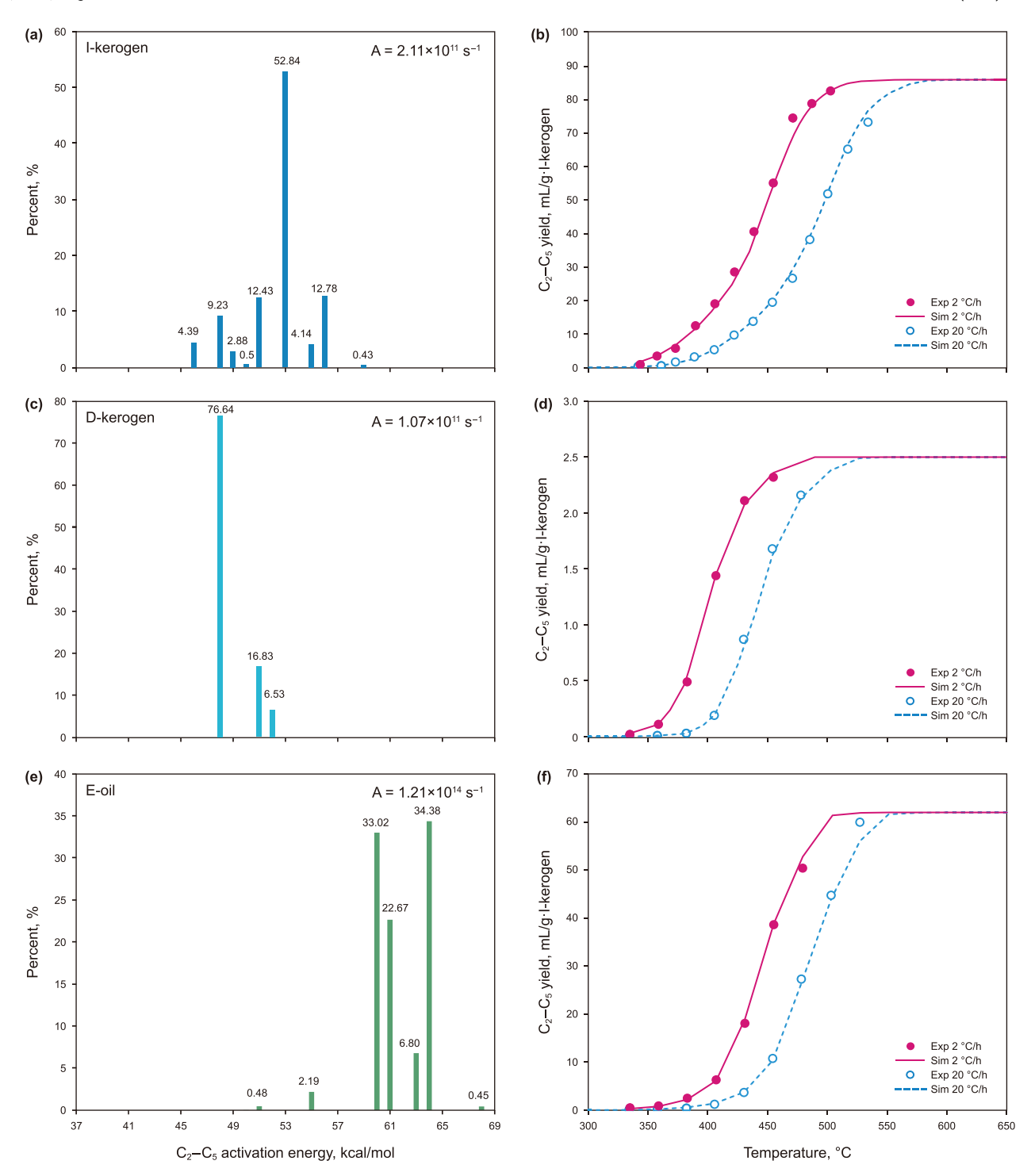


Fig. 7. Kinetic parameter distributions of  $C_2$ – $C_5$  (a, c and e) and fitting curves between the calculated and measured values of  $C_2$ – $C_5$  yield (b, d and f) from I-kerogen, D-kerogen and E-oil.

In addition, at the same pyrolysis temperature, the values of  $\delta^{13}C_1$ ,  $\delta^{13}C_2$  and  $\delta^{13}C_3$  from the E-oil were the smallest among the three pyrolysis samples. This was primarily due to the stronger isotopic fractionation effect in the oil cracking gases, resulting in products with a higher  $^{12}C$  content (Xia et al., 2013). In the low pyrolysis temperature stage,  $C_1$  and  $C_2$  from I-kerogen were more enriched in  $^{13}C$  than those from D-kerogen. However, the opposite occurred in the high pyrolysis temperature stage:  $C_1$  and  $C_2$  from I-kerogen were more enriched in  $^{12}C$  than those from D-kerogen.

Taking C<sub>1</sub> and C<sub>2</sub> at 20 °C/h as examples,  $\delta^{13}$ C<sub>1</sub> and  $\delta^{13}$ C<sub>2</sub> from I-kerogen were heavier than those from D-kerogen at temperatures below 422 °C, whereas the  $\delta^{13}$ C<sub>1</sub> and  $\delta^{13}$ C<sub>2</sub> values from I-kerogen were lighter than those from D-kerogen at temperatures above 422 °C. For  $\delta^{13}$ C<sub>3</sub>, the evolutionary trend was less clear for I-kerogen and D-kerogen due to the lack of data at low temperatures. In addition, the gas carbon isotopes exhibited a positive sequence distribution of  $\delta^{13}$ C<sub>1</sub> <  $\delta^{13}$ C<sub>2</sub> <  $\delta^{13}$ C<sub>3</sub>, such as the heavy hydrocarbon gases from I-kerogen, in the range of 388.8–533.9 °C, the difference

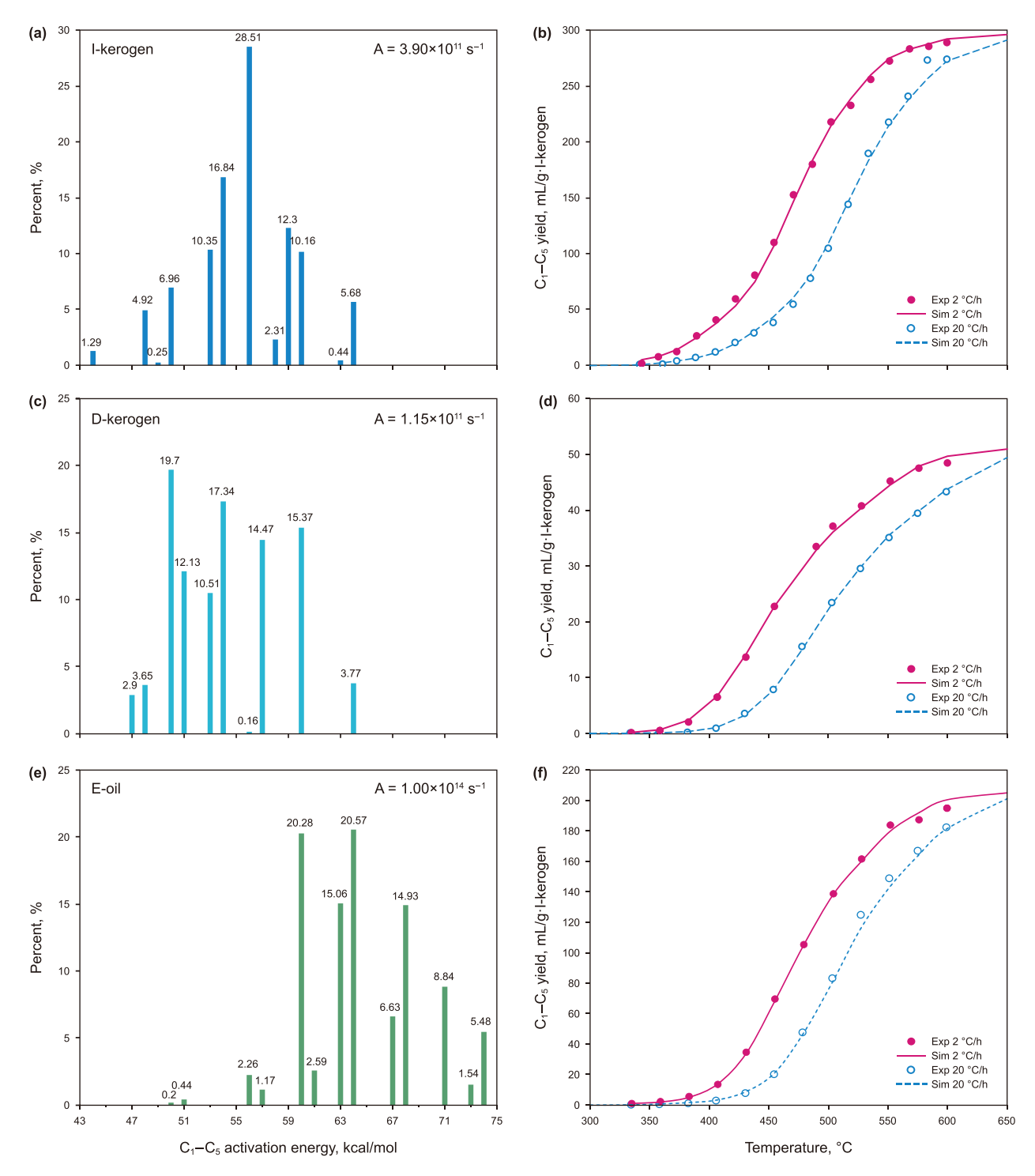


Fig. 8. Kinetic parameter distributions of  $C_1$ – $C_5$  (a, c and e) and the fitting curve between the calculated and measured values of the  $C_1$ – $C_5$  yield (b, d and f) from I-kerogen, D-kerogen and E-oil.

between  $\delta^{13}C_1$  and  $\delta^{13}C_2$  ranged from 10.43‰ to 13.08‰ and that between  $\delta^{13}C_2$  and  $\delta^{13}C_3$  ranged from 0.09‰ to 8.35‰.

## 4.5. Burial history and geothermal history

To study the gaseous hydrocarbon generated by the mudstones from the Wenchang Formation in Wenchang A Depression, a representative well (L-4) was selected to reconstruct the burial

and geothermal history using PetroMod (1D) modelling software (Fig. 10). The paleo-temperature and  $R_0$  values of the Wenchang Formation were 216–268 °C and 2.5%–4.2%, respectively.

The fitting between the measured  $R_{\rm o}$  and BHT values and the simulated  $R_{\rm o}$  and palaeotemperature curves obtained using PetroMod (1D) modelling software was good, indicating that the reconstructed burial and palaeotemperature histories were reliable.

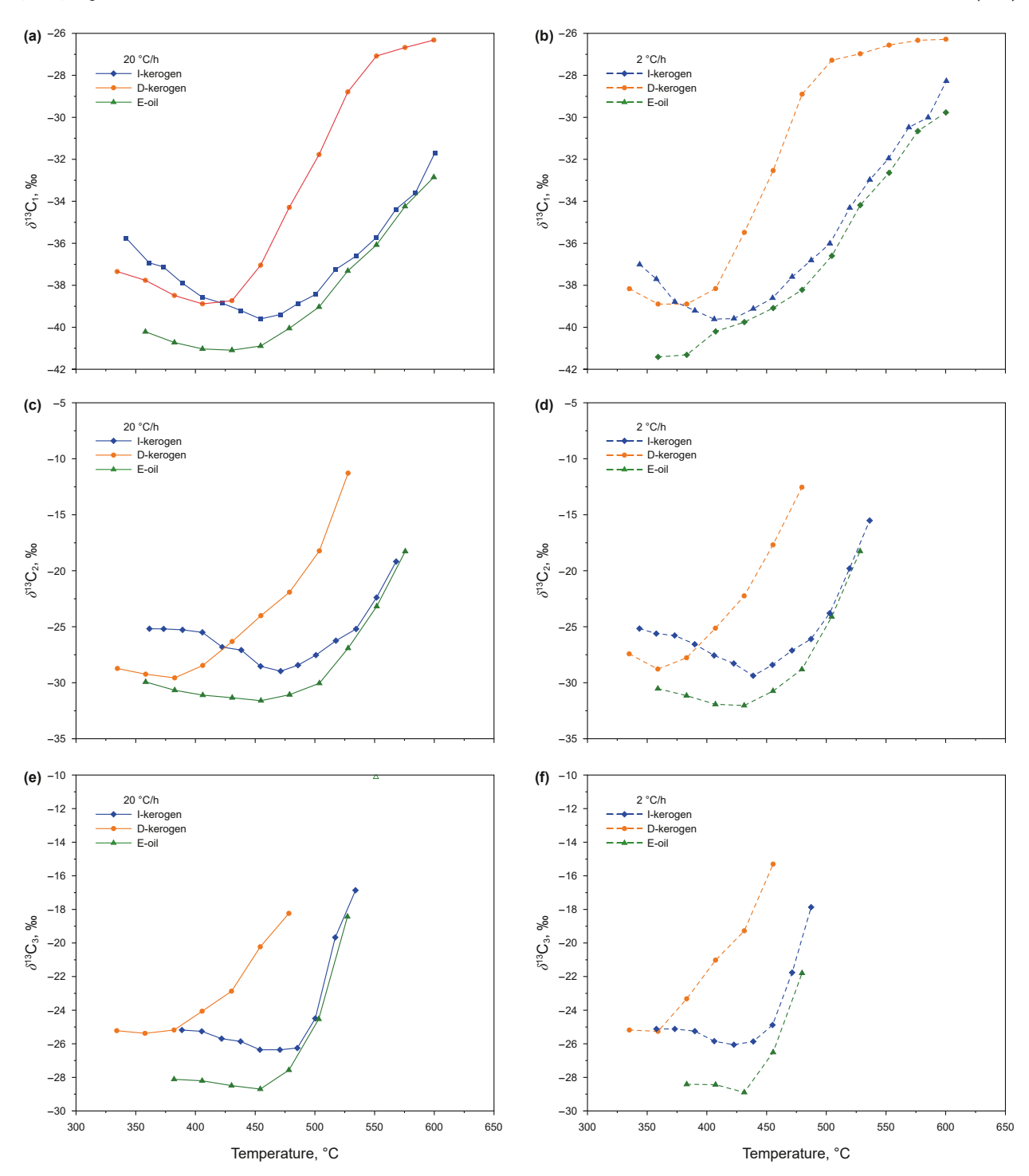


Fig. 9. Variations in the carbon isotope values of  $C_1$ ,  $C_2$  and  $C_3$  with increasing temperatures at heating rates of 20  $^{\circ}C/h$  (a, c and e), and 2  $^{\circ}C/h$  (b, d and f).

## 5. Discussion

## 5.1. Hydrocarbon generation potential

Organic matter contained in source rocks provides the material basis for the formation of oil and gas and is the main factor determining the hydrocarbon generation ability of the source rocks (Tissot and Welte, 1984; Espitalié et al., 1985). TOC, S1  $\pm$  S2 and HI are typically used to evaluate the hydrocarbon generation potential of source rocks.

Plots of HI versus  $T_{\rm max}$  (Mukhopadhyay et al., 1995; Hunt, 1996) and S2 versus TOC (Hunt, 1991; Pepper and Corvi, 1995) were used to effectively determine the organic matter type of the source rocks. The two plots showed that the studied mudstones fell in the type I and II regions, indicating that the mudstone samples from the Wenchang Formation contained type I and II organic matter (Figs. 11 and 12). Additionally, the HI values (410.71–736.17 mg/g·TOC) place them in oil-prone and very-oil-prone regions, indicating that mudstones from the Wenchang Formation have strong oil generation potential.

**Table 4**Stable carbon isotope ratios of C<sub>1</sub>, C<sub>2</sub> and C<sub>3</sub> generated from I-kerogen, D-kerogen and E-oil.

	I-keroge	en			D-kerog	gen			E-oil				
Heating rate	T, °C	$\delta^{13}C_1$ , ‰	δ <sup>13</sup> C <sub>2</sub> , ‰	δ <sup>13</sup> C <sub>3</sub> , ‰	T, °C	$\delta^{13}C_1$ , ‰	$\delta^{13}C_2$ ,‰	δ <sup>13</sup> C <sub>3</sub> , ‰	T, °C	$\delta^{13}C_1$ , ‰	δ <sup>13</sup> C <sub>2</sub> , ‰	δ <sup>13</sup> C <sub>3</sub> , ‰	
20 °C/h	341.8	-35.74			334.4	-37.34	-28.72	-25.21	334.4				
	361.1	-36.92	-25.16		358.0	-37.76	-29.23	-25.37	358.0	-40.21	-29.92		
	373.0	-37.12	-25.18		382.3	-38.48	-29.56	-25.17	382.3	-40.73	-30.66	-28.11	
	388.8	-37.89	-25.26	-25.17	405.7	-38.88	-28.45	-24.05	405.7	-41.03	-31.10	-28.20	
	405.4	-38.56	-25.48	-25.25	430.3	-38.73	-26.31	-22.86	430.3	-41.09	-31.33	-28.49	
	422.0	-38.85	-26.81	-25.69	454.3	-37.04	-24.00	-20.21	454.3	-40.89	-31.60	-28.69	
	437.9	-39.20	-27.07	-25.85	478.3	-34.28	-21.89	-18.22	478.3	-40.05	-31.06	-27.56	
	454.0	-39.60	-28.52	-26.35	503.2	-31.76	-18.20		503.2	-39.03	-30.04	-24.52	
	470.8	-39.39	-28.96	-26.35	527.2	-28.77	-11.25		527.2	-37.31	-26.90	-18.41	
	485.3	-38.87	-28.42	-26.25	551.1	-27.06			551.1	-36.07	-23.16		
	500.3	-38.43	-27.52	-24.48	575.0	-26.65			575.0	-34.23	-18.24		
	517.0	-37.24	-26.23	-19.65	599.1	-26.30			599.1	-32.84			
	533.9	-36.61	-25.19	-16.84									
	551.0	-35.72	-22.37										
	567.3	-34.37	-19.15										
	583.5	-33.60											
	599.9	-31.68											
2 °C/h	343.6	-37.00	-25.13		335.0	-38.16	-27.39	-25.17	335.0				
	357.6	-37.70	-25.58	-25.11	359.0	-38.89	-28.75	-25.25	359.0	-41.41	-30.50		
	373.0	-38.78	-25.75	-25.11	383.0	-38.89	-27.74	-23.31	383.0	-41.31	-31.13	-28.41	
	389.8	-39.20	-26.53	-25.24	407.1	-38.15	-25.09	-21.01	407.1	-40.20	-31.90	-28.43	
	406.0	-39.61	-27.53	-25.84	431.1	-35.47	-22.21	-19.26	431.1	-39.75	-32.01	-28.89	
	422.4	-39.58	-28.25	-26.05	455.2	-32.52	-17.64	-15.28	455.2	-39.08	-30.71	-26.50	
	438.6	-39.11	-29.35	-25.86	479.4	-28.88	-12.49		479.4	-38.21	-28.78	-21.78	
	454.7	-38.60	-28.38	-24.87	504.3	-27.26			504.3	-36.59	-24.07		
	471.1	-37.59	-27.09	-21.75	528.0	-26.95			528.0	-34.17	-18.21		
	487.0	-36.80	-26.06	-17.85	552.1	-26.54			552.1	-32.63			
	502.6	-36.00	-23.75		576.1	-26.31			576.1	-30.64			
	519.2	-34.30	-19.75		599.6	-26.26			599.6	-29.75			
	536.0	-32.96	-15.47										
	551.8	-31.94											
	568.6	-30.46											
	584.7	-29.99											
	600.0	-28.25											

Based on the magnitude of S1 + S2 and TOC values, Peters and Cassa (1994) and Hakimi et al. (2010) classified the hydrocarbon generation potential of source rocks into five levels: poor (TOC < 0.5% and S1 + S2 < 2 mg/g), fair (TOC = 0.5%–1.0% and S1 + S2 = 2–6 mg/g) good (TOC = 1%–2% and S1+S2 = 6–10 mg/g), very good (TOC = 2%–4% and S1 + S2 = 10–22 mg/g), and excellent (TOC > 4% and S1 + S2 > 22 mg/g). The TOC and S1 + S2 values of the samples in the present study mostly ranged from 1.42% to 3.12% and 9.71 mg/g to 20.61 mg/g, respectively, and the plot of S1 + S2 versus TOC showed that most of the mudstones from the Wenchang Formation were good to very good source rocks (Fig. 13).

## 5.2. Gas source identification

Based on the geochemical characteristics of natural gas generated from source rocks of different organic matter types, various natural gas composition indicators and plots have been used to identify gases obtained from the primary cracking of kerogen or the secondary cracking of oil (Prinzhofer et al., 2000; Cramer, 2004; Dai et al., 2017).

In the plot of  $\delta^{13}C_2 - \delta^{13}C_3$  versus  $\ln(C_2/C_3)$  (Fig. 14(a)), the gases produced from D-kerogen and E-oil were clearly separate due to their distinct evolutionary trends. The  $\delta^{13}C_2 - \delta^{13}C_3$  values of gas from D-kerogen showed minimal variation, ranging from -2.95% to -4.5%. However, the  $\ln(C_2/C_3)$  values showed large variations ranging from 1.4 to 2.65, exhibiting a sub-horizontal line. The  $\delta^{13}C_2 - \delta^{13}C_3$  values of gas from E-oil showed large variations of -2.55% to -8.49%, whereas the variation in  $\ln(C_2/C_3)$  was

small at 0.22 to 0.63, exhibiting a sub-vertical line. As shown in Fig. 14(b), the gases produced from D-kerogen and E-oil had a similar evolutionary trend to  $\delta^{13}C_2 - \delta^{13}C_3$  versus  $\ln(C_2/C_3)$ : increasing  $\delta^{13}C_1$  values, and slight increases in  $\delta^{13}C_2$ – $\delta^{13}C_3$  for the D-kerogen derived gases (exhibiting a sub-horizontal line) but rapid decreases for E-oil derived gases (exhibiting a sub-vertical line). However, certain data overlap indicated that two types of gases in the plot of  $\delta^{13}C_2 - \delta^{13}C_3$  versus  $\delta^{13}C_1$  could not be effectively separated. Similarly, in the plots of  $ln(C_2/C_3)$  versus  $ln(C_1/C_2)$ (Fig. 14(c)) and  $\delta^{13}C_1 - \delta^{13}C_2$  versus  $ln(C_1/C_2)$  (Fig. 14(d)), although the gases generated by D-kerogen and E-oil exhibited different evolutionary trends, there was a data overlap phenomenon (indicated by the yellow shaded area in the figure). Compared with the parameters  $ln(C_1/C_2)$ ,  $\delta^{13}C_1$ – $\delta^{13}C_2$  and  $\delta^{13}C_1$ , the gaseous hydrocarbons from the primary cracking of kerogen and the secondary cracking of oil are more sensitive to changes in  $\delta^{13}C_2 - \delta^{13}C_3$ and  $\ln(C_2/C_3)$  values. Therefore, the plot of  $\delta^{13}C_2 - \delta^{13}C_3$  versus ln  $(C_2/C_3)$  effectively distinguished the origin of the gas, while the other three plots (Fig. 14(b), (c) and (d)) were not entirely effective. This further indicates the  $C_{2+}$  fraction is more reliable than the  $C_1$ fraction as a genetic signature of a gas (Prinzhofer and Lorant, 1997; Prinzhofer et al., 2000).

In addition, the evolutionary trend of the I-kerogen gas was similar to that of E-oil within four gas source identification plots, showing that the gaseous hydrocarbon generated by the oil-prone mudstones was mainly derived from the secondary cracking of oil; this is consistent with previous results showing that gaseous hydrocarbons generated by I- and II-kerogen are mostly derived from the secondary cracking of oil (Behar et al., 1995; Zeng, 2020).

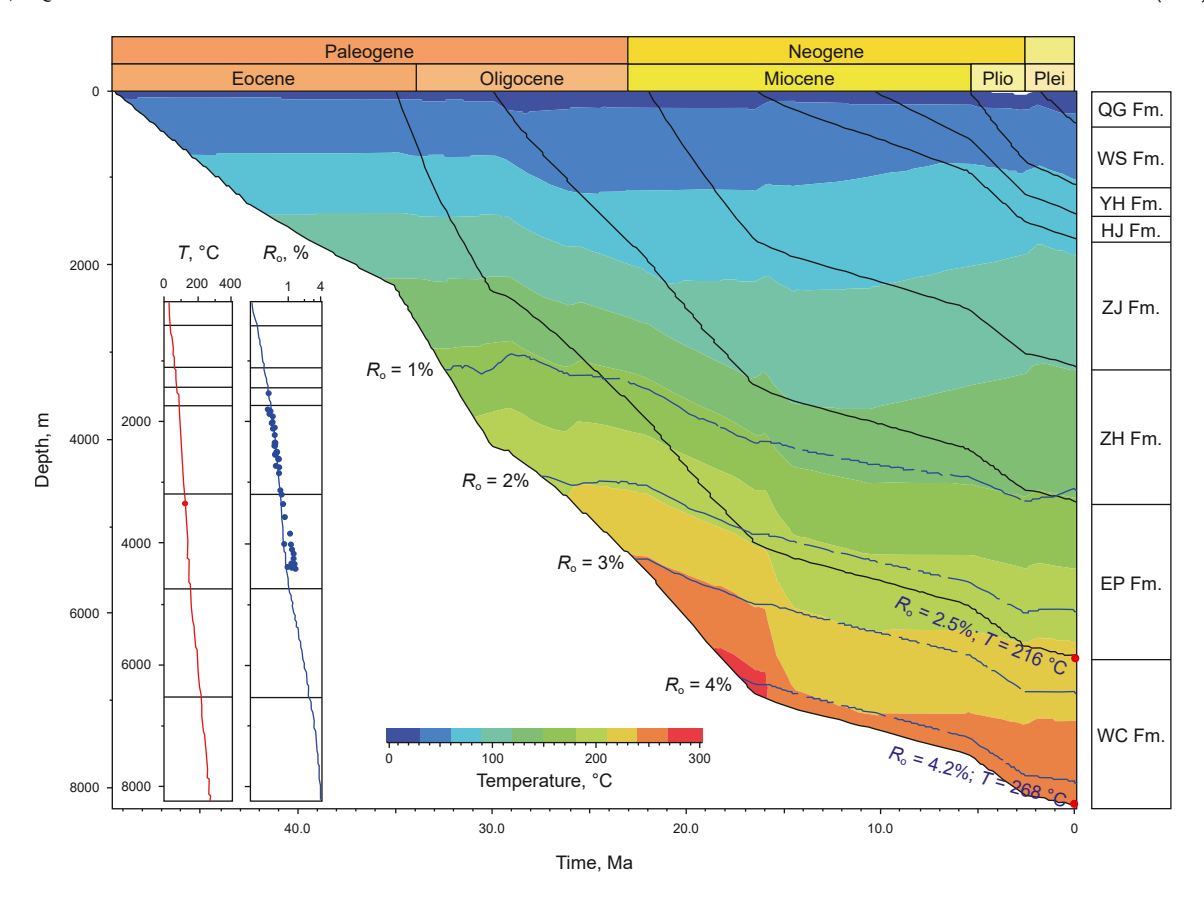


Fig. 10. Diagram showing burial and geothermal history of L-4 well in the Wenchang A Depression from the Paleogene to the present.

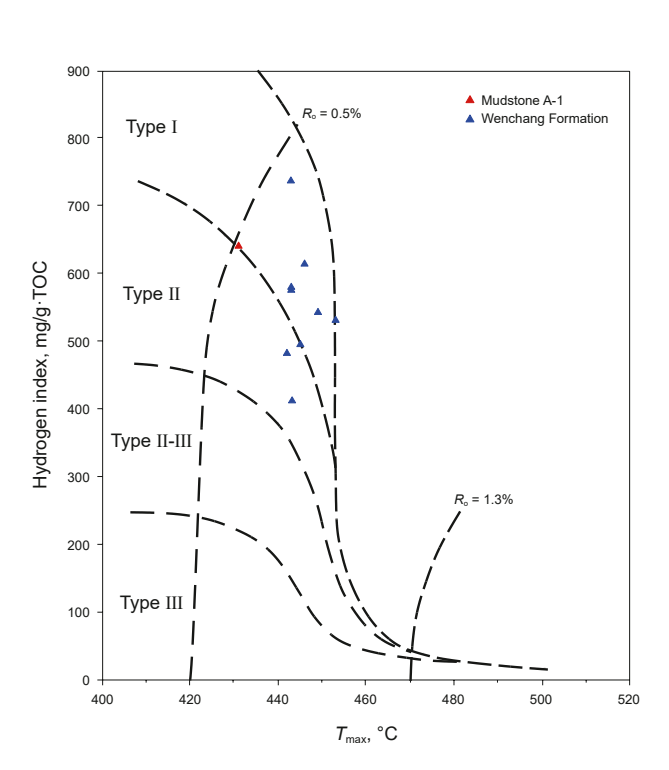


Fig. 11. Plot of HI versus  $T_{\rm max}$  for mudstones from the Wenchang Formation in the Wenchang A Depression.

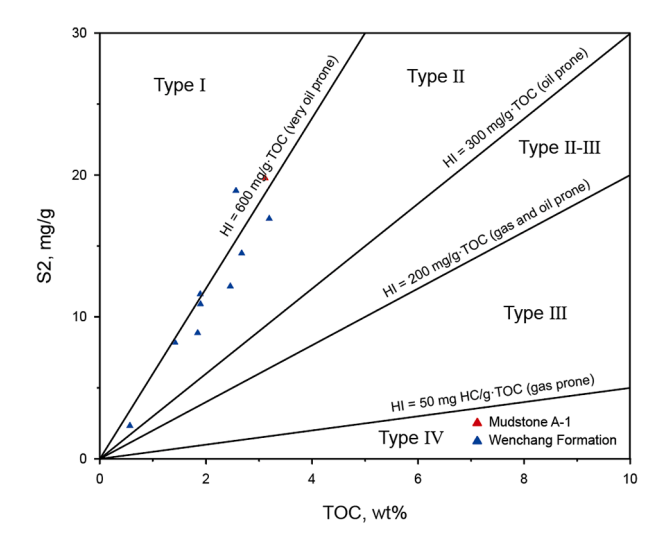


Fig. 12. Plot of S2 versus TOC for mudstones from the Wenchang Formation in the Wenchang A Depression.

# 5.3. Process of gaseous hydrocarbon generation under geological conditions

The process of hydrocarbon generation from source rocks is complicated, and the exact yields of oil and gas generated from source rocks cannot be determined from simple observations of natural samples (Behar et al., 1992; Price and Wenger, 1992; Pan et al., 2012). Thermal simulation experiments and a wealth of petroleum exploration data indicate that the hydrocarbon

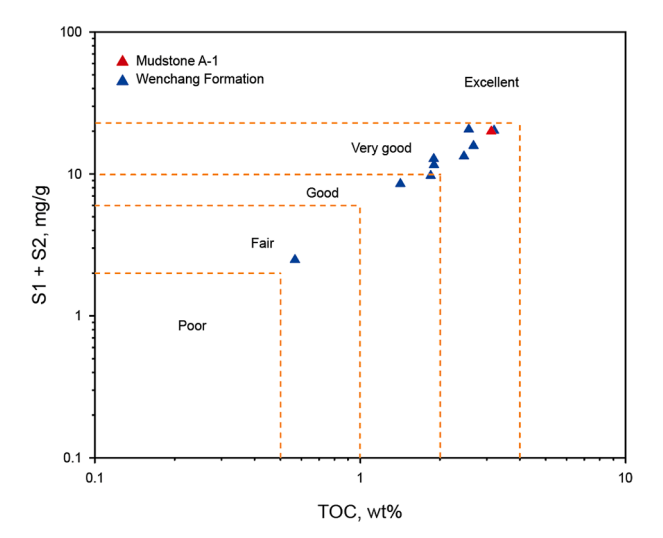


Fig. 13. Plot of S1  $\pm$  S2 versus TOC for mudstones from the Wenchang Formation within the Wenchang A Depression.

formation process can be ascertained by integrating a kinetic model with geothermal history under real geological settings (Tissot et al., 1987; Ungerer and Pelet, 1987; Sweeney and Burnham, 1990; Peters et al., 2018). In this study, we applied the

kinetic parameters of the I-kerogen, D-kerogen and E-oil to the burial geological conditions of the Wenchang A Depression from the Zhu III Sub-basin in the Pearl River Mouth Basin (PRMB). We then reconstructed the gases generation process of mudstones from the Wenchang Formation.

To illustrate the ratio of gas generated from oil cracking to the gas generated from I-kerogen, the ratio of gaseous hydrocarbons ( $GR_{oil}$ ) was calculated according to Eq. (1),

$$GR_{oil} = Y_{E-oil} \div Y_{I-kerogen}$$
 (1)

where  $Y_{\text{E-oil}}$  and  $Y_{\text{I-kerogen}}$  are the gas yields generated from the oil cracking and I-kerogen, respectively.

The gaseous hydrocarbon generation process of the mudstone from the Wenchang Formation in the Wenchang A Depression is shown in Fig. 15. The gaseous hydrocarbons generated by I-kerogen, D-kerogen and E-oil began at approximately 33 Ma. For C<sub>1</sub> generation from I-kerogen and E-oil cracking, there were two distinct turning points at 22 Ma and 16 Ma (Fig. 15(a)); the C<sub>1</sub> yield of these two samples increased significantly from 22 Ma to 16 Ma, and then began to increase slowly after 16 Ma. To date, the C<sub>1</sub> yields have reached 232.03 mL/g·I-kerogen and 145.91 mL/g·I-kerogen, respectively. The yield of C<sub>2</sub>–C<sub>5</sub> generated from E-oil was much higher than that generated from D-kerogen (Fig. 15(b)), with GR<sub>0il</sub> values of C<sub>2</sub>–C<sub>5</sub> ranging from 65% to 81% (Fig. 15(d)),

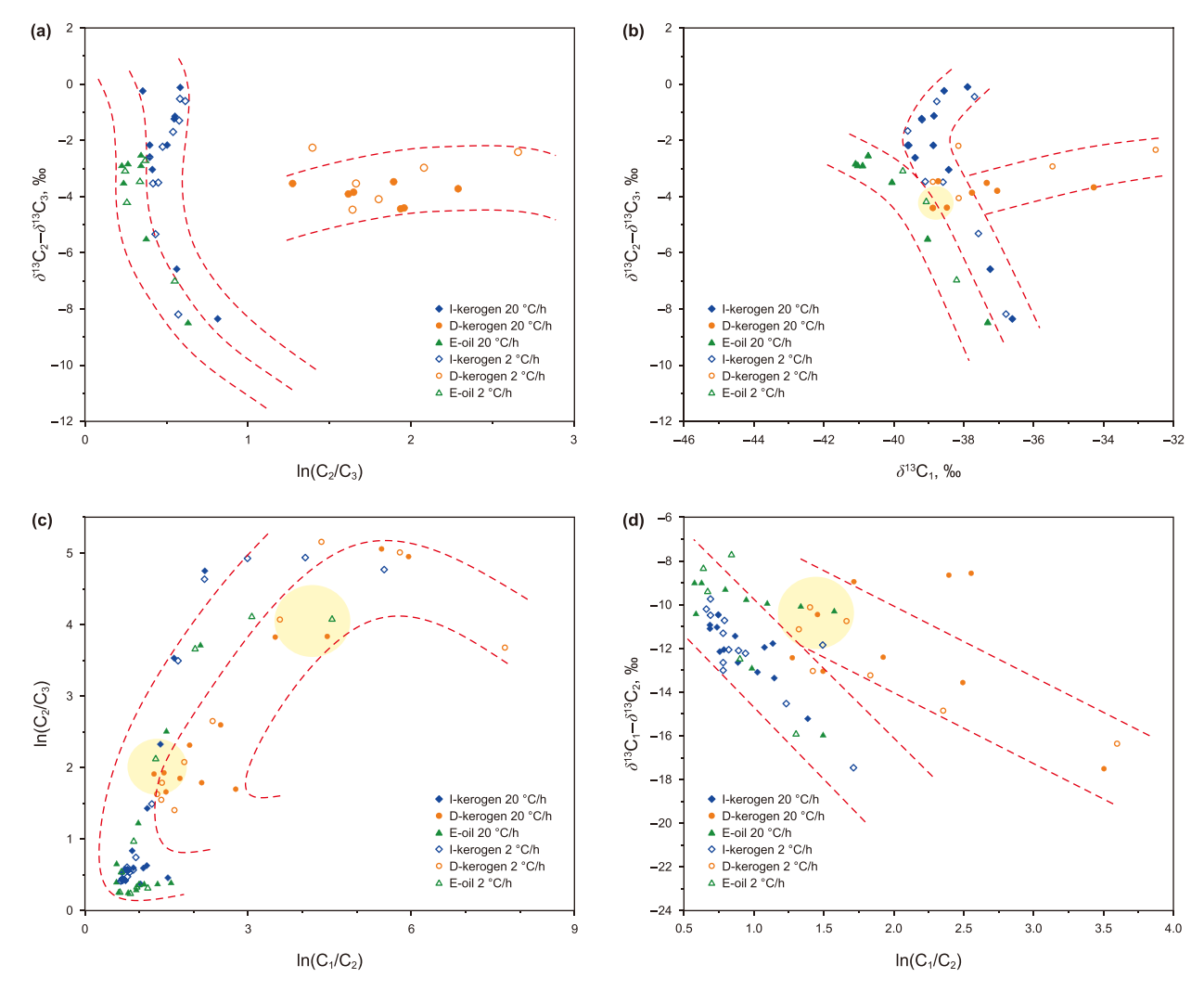


**Fig. 14.** Gas source identification plots. (a)  $\ln(C_2/C_3)$  versus  $\delta^{13}C_2$ — $\delta^{13}C_3$ , modified from Prinzhofer and Huc (1995); (b) plot of  $\delta^{13}C_1$  versus  $\delta^{13}C_2$ — $\delta^{13}C_3$ , modified from Tian (2006); (c)  $\ln(C_2/C_3)$  versus  $\ln(C_1/C_2)$ , modified from Lorant et al. (1998) and (d)  $\delta^{13}C_1$ — $\delta^{13}C_2$  versus  $\ln(C_1/C_2)$ , modified from Jenden et al. (1993).

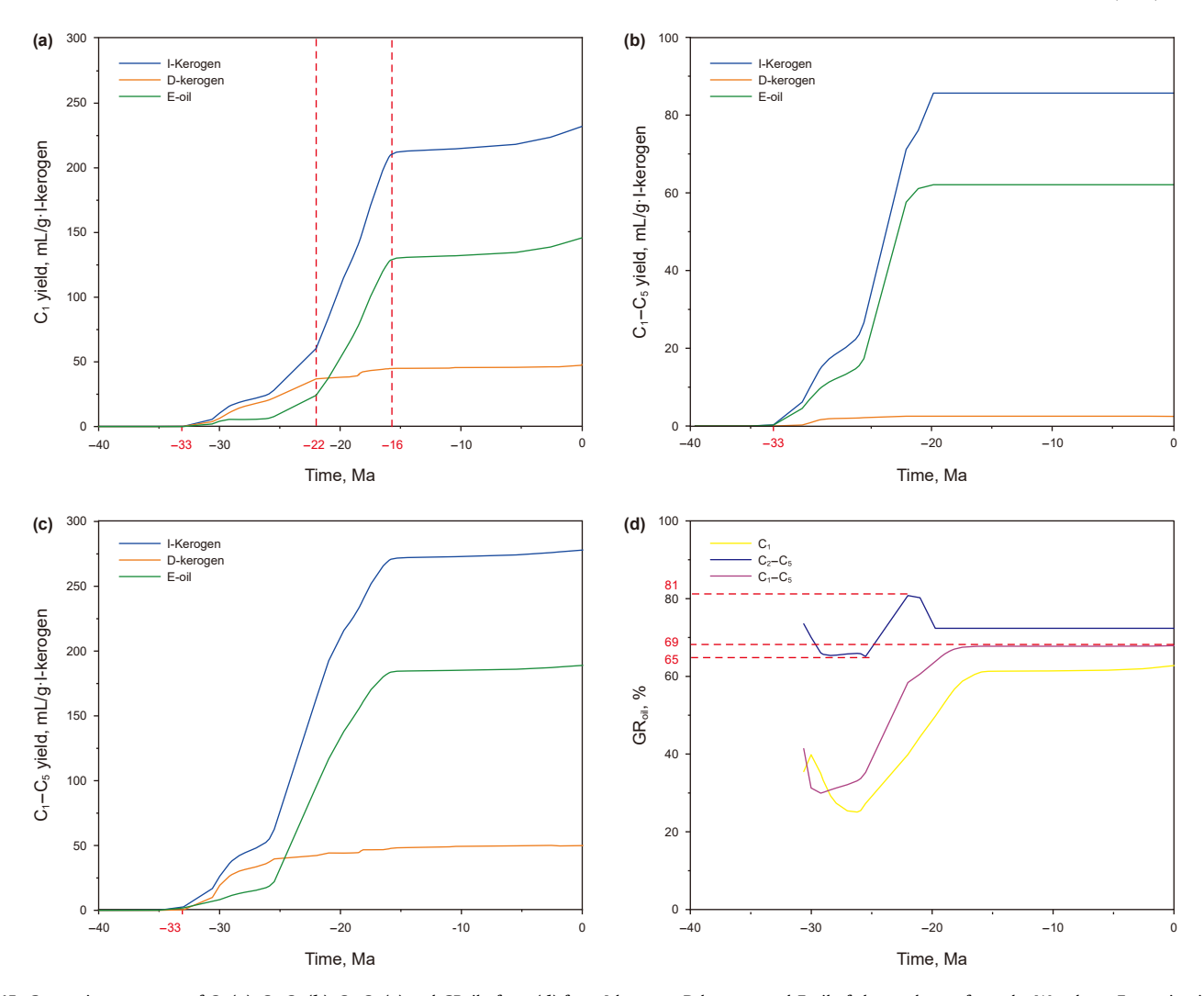


Fig. 15. Generation processes of  $C_1$  (a),  $C_2$ – $C_5$  (b),  $C_1$ – $C_5$  (c) and GRoil of gas (d) from I-kerogen, D-kerogen and E-oil of the mudstone from the Wenchang Formation in the Wenchang A Depression.

indicating that the  $C_2$ – $C_5$  generated by mudstones from the Wenchang Formation is mainly derived from oil cracking. This agrees with past research (Guo et al., 2009; Tian et al., 2010) showing that the primary cracking of oil-prone kerogen contributes little to the  $C_2$ – $C_5$  content, primarily because primary and secondary oil cracking have different gas-generation mechanisms. Kerogen cracking gases mainly originate from demethylation or dealkylation reactions and contain a small amount of heavy hydrocarbon gases, whereas oil cracking gases are mainly related to the depolymerization reactions of non-hydrocarbons and the C–C bond cracking of  $C_{6+}$  saturates, and they contain large amounts of heavy hydrocarbon gas (Behar et al., 1999; Lorant et al., 2000). The maximum  $G_{0il}$  of the  $C_1$ – $C_5$  was 69% (Fig. 15(d)), which is slightly lower than the maximum value (75%) in Burnham's (1989) type-I kerogen gas generation model.

#### 6. Conclusions

1) Mudstones from the Wenchang Formation contain type I and II organic matter, with TOC ranging from 0.57% to 3.20%, S1 + S2 from 9.71 to 20.61 mg/g and HI from 410.71 to 736.17 mg/g-TOC, respectively. These mudstones are oil-prone, classified as good

- to very good source rocks, and exhibit strong oil generation potential.
- 2) The plots of  $\ln(C_2/C_3)$  versus  $\delta^{13}C_2 \delta^{13}C_3$  can effectively distinguish the origin of the gases. Oil cracking gas is the primary source of gaseous hydrocarbons generated from mudstone in the Wenchang Formation.
- 3) The gaseous hydrocarbon generation from the mudstones began at approximately 33 Ma, with a maximum of 69% of total gaseous hydrocarbons (C<sub>1</sub>–C<sub>5</sub>) generated by oil cracking. The total heavy hydrocarbon gases (C<sub>2</sub>–C<sub>5</sub>) generated are mainly derived from oil cracking, accounting for 65%–81%.

## **CRediT authorship contribution statement**

**Shu-Xia Li:** Writing – original draft, Software, Methodology. **Bin Xu:** Writing – original draft, Funding acquisition, Data curation. **Shu-Qian Li:** Software, Resources, Formal analysis. **Feng-Hua Zhao:** Visualization, Supervision, Investigation, Funding acquisition. **You-Chuan Li:** Supervision, Resources. **Hong-Fu Sun:** Validation, Resources. **Le Lu:** Visualization, Resources. **Jin-Zhong Liu:** Writing – review & editing, Supervision, Data curation, Conceptualization.

#### **Declaration of competing interest**

We declare that we have no financial and personal relationships with other people or organizations that can inappropriately influence our work, there is no professional or other personal interest of any nature or kind in any product, service and/or company that could be construed as influencing the position presented in, or the review of, the manuscript entitled.

## Acknowledgements

This study was supported by the Central Young College Teachers Fund Project of China (Grant No.3142020002), the Fundamental Research Funds for the Central Universities (Grant No.3142021004), the National Natural Science Foundation of China (Grant No. 41673066 and No.42202291) and the Construction of the Water Damage Model in the Xishan Coal Power Mining Area (Grant No. 20230767).

## References

- Behar, F., Budzinski, H., Vandenbroucke, M., et al., 1999. Methane generation from oil cracking: kinetics of 9-methylphenanthrene cracking and comparison with other pure compounds and oil fractions. Energy Fuel. 13, 471–481. https://doi.org/10.1021/ef980164n
- Behar, F., Vandenbroucke, M., Tang, Y., et al., 1997. Thermal cracking of kerogen in open and closed systems: determination of kinetic parameters and stoichiometric coefficients for oil and gas generation. Org. Geochem. 5, 321–339. https://doi.org/10.1016/S0146-6380(97)00014-4.
- Behar, F.S., Kressmann, S., Rudkiewicz, J.L., et al., 1992. Experimental simulation in a confined system and kinetic modelling of kerogen and oil cracking. Org. Geochem. 19, 173–189. https://doi.org/10.1016/0146-6380(92)90035-V.
- Behar, F., Vandenbroucke, M., Teermann, S.C., et al., 1995. Experimental simulation of gas generation from coals and a marine kerogen. Chem. Geol. 126 (3–4), 247–260. https://doi.org/10.1016/0009-2541(95)00121-2.
- Berner, U., Faber, E., Scheeder, G., et al., 1995. Primary cracking of algal and landplant kerogens: kinetic models of isotope variations in methane, ethane and propane. Chem. Geol. 126, 233–245. https://doi.org/10.1016/0009-2541(95)
- Burnham, A.K.. A simple kinetic model of petroleum formation and cracking. https://www.researchgate.net/publication/236379291.
- Burnham, A.K., Braun, R.L., 1999. Global kinetic analysis of complex materials. Energy Fuel. 13, 1–22. https://doi.org/10.1021/ef9800765.
- Cai, Q.Z., 2005. Oil and Gas Geology in China Seas. Ocean Press, Beijing (in Chinese). Cheng, P., Xiao, X.M., Gai, H.F., et al., 2015. Characteristics and origin of carbon isotopes of n-alkanes in crude oils from the western Pearl River Mouth Basin, South China Sea. Mar. Petrol. Geol. 67, 217–229. https://doi.org/10.1016/j.marpetgeo.2015.05.028.
- Cheng, P., Xiao, X.M., Tian, H., et al., 2013. Source controls on geochemical characteristics of crude oils from the Qionghai Uplift in the western Pearl River Mouth Basin, offshore South China Sea. Mar. Petrol. Geol. 40, 85–98. https://doi.org/10.1016/j.marpetgeo.2012.10.003.
- Cramer, B., 2004. Methane generation from coal during open system pyrolysis investigated by isotope specifc, Gaussian distributed reaction kinetics. Org. Geochem. 35, 379–392. https://doi.org/10.1016/j.orggeochem.2004.01.004.
- Dieckmann, V., Schenk, H.J., Horsfield, B., et al., 1998. Kinetics of petroleum generation and cracking by programmed-temperature closed-system pyrolysis of Toarcian Shales. Fuel 77 (1), 23–31. https://doi.org/10.1016/s0140-6701(98) 97240-x.
- Dai, J.X., Ni, Y.Y., Gong, D.Y., et al., 2017. Geochemical characteristics of gases from the largest tight sand gas field (Sulige) and shale gas field (Fuling) in China. Mar. Petrol. Geol. 79, 426–438. https://doi.org/10.1016/j.marpetgeo.2016.10.021.
- Espitalié, J., Deroo, G., Marquis, F., 1985. Rock-Eval pyrolysis and its applications (Part Two). Rev. IF Petrol. 40 (6), 755–784. https://doi.org/10.2516/ogst: 1985045
- Espitalié, J., Ungerer, P., Irwin, I., et al., 1988. Primary cracking of kerogens. Experimenting and modelling C<sub>1</sub>, C<sub>2</sub>-C<sub>5</sub>, C<sub>6</sub>-C<sub>15</sub> and C<sub>15+</sub> classes of hydrocarbons formed. Org. Geochem. 13, 893–899. https://doi.org/10.1016/0146-6380 (88)90243-4
- Fu, N., Li, Y.C., Sun, J.X., et al., 2011. Recognition of oil source and source rocks in Zhu III depression. Geoscience 25, 1121–1130. https://doi.org/10.1016/S1003-9953(10)60145-4 (in Chinese).
- Gan, H.J., 2007. Accumulation history and formation mechanism of petroleum pools in Wenchang A sag, western Pearl River Mouth Basin. Guangzhou Institute of Geochemistry. Chinese Academy of Sciences, p. 105 (in Chinese).
- Gan, H.J., Tian, H., Huang, B.J., et al., 2009. Generation and accumulation of oil and condensates in the Wenchang A Sag, western Pearl River Mouth Basin, South China Sea. Geofluids 9, 275–286. https://doi.org/10.1111/j.1468-8123.2009.00264.x.

Gan, J., Zhang, Y.C., Deng, Z.Y., et al., 2012. Reservoir-forming characteristic and model of the palaeogene condensate gas reservoir with low permeability in Wenchang A Sag. Nat. Gas Geosci. 23 (6), 1060–1069 doi:CNKI:SUN: TDKX.0.2012-06-013. (in Chinese).

- Ga, Y.D., Liu, J., Peng, G.R., et al., 2024. New fields and resource potential of oil and gas exploration in Pearl River Mouth Basin. Acta Pet. Sin. 45 (1), 183–201. https://doi.org/10.7623/syxb202401011 (in Chinese).
- Gong, Z.S., Li, S.T., 2004. Dynamic Research of Oil and Gas Accumulation in Northern Marginal Basins of South China Sea. Science Press, Beijing, pp. 1–339 (in Chinese).
- Guo, L.G., Xiao, X.M., Tian, H., et al., 2009. Distinguishing gases derived from oil cracking and kerogen maturation: insights from laboratory pyrolysis experiments. Org. Geochem. 40, 1074–1084. https://doi.org/10.1016/j.orggeochem.2009.07.007.
- Hakimi, M.H., Abdulah, W.H., Shalaby, M.R., 2010. Organic geochemistry, burial history and hydrocarbon generation modelling of the Upper Jurassic Madbi Formation, Masila Basin, Yemen. J. Petrol. Geol. 4, 299–318. https://doi.org/ 10.1111/j.1747-5457.2010.00481.x.
- Hill, R.J., Tang, Y., Kaplan, I.R., 2003. Insights into oil cracking based on laboratory experiments. Org. Geochem. 34, 1651–1672. https://doi.org/10.1016/S0146-6380(03)00173-6.
- He, Z.T., Yin, X.D., Lei, M.Z., et al., 2024. Origin of the abnormal carbon isotopic in organic matter of the Wenchang Formation, Zhu III sub-basin, Pearl River Mouth Basin. Acta Geol. Sin. 98 (1), 266–279. https://doi.org/10.19762/j.cnki.dizhixuebao.2023038 (in Chinese).
- He, K., Zhang, S.C., Mi, J.K., et al., 2018. The evolution of chemical groups and isotopic fractionation at different maturation stages during lignite pyrolysis. Fuel 211, 492–506. https://doi.org/10.1016/j.fuel.2017.09.085.
- Hu, G.Y., Xiao, Z.Y., Luo, X., et al., 2005. Light hydrocarbon composition difference between two kinds of cracked gases and its application. Nat. Gas. Ind. 25, 23–25. https://doi.org/10.1360/gs050303 (in Chinese).
- Huang, B.J., Li, J.L., Li, L., et al., 2007. A discussion on the hydrocarbon accumulation characteristics and distribution in Wenchang A sag. China Offshore Oil Gas, 361–366. https://doi.org/10.3969/j.issn.1673-1506.2007.06.001 (in Chinese).
- Huang, B.J., Xiao, X.M., Zhang, M.Q., 2003. Geochemistry, grouping and origins of crude oils in the Western Pearl River Mouth Basin, offshore South China Sea. Org. Geochem. 34, 993–1008. https://doi.org/10.1016/S0146-6380(03)00035-4.
- Hunt, J.M., 1996. Petroleum Geochemistry and Geology. WH Freeman and Co, New York.
- Hunt, J.M., 1991. Generation of gas and oil from coal and other terrestrial organic matter. Org. Geochem. 17, 673–680. https://doi.org/10.1016/0146-6380(91) 90011-8.
- Jiang, H., Wang, H., Li, J.L., et al., 2009. Research on hydrocarbon pooling and distribution patterns in the Zhu-3 Depression, the Pearl River Mouth Basin. Oil Gas Geol. 30, 275–281+286. https://doi.org/10.11743/ogg20090304 (in Chinese).
- Jenden, P.D., Drazan, D.J., Kaplan, I.R., 1993. Mixing of thermogenic natural gases in Northern Appalachian Basin. American Association of Petroleum Geologists Bulletin 77, 980–998. https://doi.org/10.1029/93GL01454.
- Ji, H.Q., Wang, X.H., 2004. The potential of oil and gas exploration in Wenchang A Sag of the Pearl River Mouth Basin. Nat. Gas Geosci. (3), 238–242. https://doi. org/10.3969/j.issn.1672-1926.2004.03.007 (in Chinese).
- Li, S.X., Shao, L.Y., Liu, J.S., et al., 2022. Oil generation model of the liptinite-rich coals: Palaeogene in the Xihu Sag, East China Sea Shelf Basin. J. Petrol. Sci. Eng. 209, 109844. https://doi.org/10.1016/j.petrol.2021.109844.
- Li, J.H., Chen, D.X., Chang, L., et al., 2020. Quality, hydrocarbon generation, and expulsion of the Eocene Enping Formation source rocks in the Wenchang depression, western Pearl River Mouth Basin, South China Sea. Energy Explor. Exploit. 38, 2169–2198. https://doi.org/10.1177/0144598720915583.
- Liu, J.P., Wang, L.L., Xiaoling, J., et al., 2015. Analyzing geochemical characteristics and hydrocarbon generation history of the Middle and upper Jurassic source rocks in the North Yellow Sea Basin. J. Pet. Sci. Eng. 126, 141–151. https://doi. org/10.1016/j.petrol.2014.10.003.
- Liu, J.Z., Tang, Y.C., 1998. One example of predicting methane generation yield by hydrocarbon generating kinetics. Chin. Sci. Bull. 43, 1187–1191. https://doi.org/ 10.1360/csb1998-43-11-1187.
- Liu, Y., Xu, Z.M., Lei, M.Z., et al., 2022. Organic geochemical characteristics of Enping Formation source rocks in Wenchang A sag, Pearl River Mouth Basin, China. Arabian J. Geosci. 15, 316. https://doi.org/10.1007/S12517-022-09584-4.
- Lorant, F., Behar, F., Vandenbroucke, M., et al., 2000. Methane generation from methylated aromatics: kinetic study and carbon isotope modeling. Energy Fuel. 14, 1143–1155. https://doi.org/10.1021/ef990258e.
- Lorant, F., Prinzhofer, A., Behar, F., et al., 1998. Carbon isotopic and molecular constraints on the formation and the expulsion of thermogenic hydrocarbon gases. Chem. Geol. 147, 249–264. https://doi.org/10.1016/S0009-2541(98) 00017-5.
- Mukhopadhyay, P.K., Wade, J.A., Kruge, M.A., 1995. Organic facies and maturation of Jurassic/Cretaceous rocks, and possible oil-source rock correlation based on pyrolysis of asphaltenes, Scotian Basin, Canada. Org. Geochem. 22, 85–104. https://doi.org/10.1016/0146-6380(95)90010-1.
- Pan, C., Jiang, L., Liu, J., et al., 2012. The effects of pyrobitumen on oil cracking in confined pyrolysis experiments. Org. Geochem. 45, 29–47. https://doi.org/ 10.1016/j.orggeochem.2012.01.008.
- Pelet, R., 1994. Comments on the paper "The effects of the mineral matrix on the determination of kinetic parameters using modified Rock-Eval pyrolysis" by H. Org. Geochem. 21, 979–981. https://doi.org/10.1016/0146-6380(94)90056-6.

Peters, K.E., Burnham, A.K., Walters, C.C., et al., 2018. Guidelines for kinetic input to petroleum system models from open-system pyrolysis. Mar. Petrol. Geol. 92, 979–986. https://doi.org/10.1016/j.marpetgeo.2017.11.024.

- Peters, K.E., Cassa, M.R., 1994. Applied source rock geochemistry. In: Magoon, Leslie B., Dow, Wallace G. (Eds.), The Petroleum System-From Source to Trap. AAPG, Tulsa. https://doi.org/10.1306/M60585C5.
- Pepper, A.S., Corvi, P.J., 1995. Simple kinetic models of petroleum formation: Part I. Oil and gas generation from kerogen. Mar. Petrol. Geol. 12, 291–319. https://doi.org/10.1016/0264-8172(95)98381-E.
- Price, L.C., Wenger, L.M., 1992. The influence of pressure on petroleum generation and maturation as suggested by aqueous pyrolysis. Org. Geochem. 19, 141–159. https://doi.org/10.1016/0146-6380(92)90033-t.
- Prinzhofer, A., Mello, M.R., Takaki, T., 2000. Geochemical characterization of natural gas: a physical multivariable approach and its applications in maturity and migration estimates: reply. AAPG Bulletin 84, 53–72. https://doi.org/10.1306/A9673C66-1738-11D7-8645000102C1865D.
- Prinzhofer, A., Lorant, F., 1997. Ethane/propane diagram for gas gen-esis characterization. In: Proceedings of the 18th International Meeting. Assosiation of Organic Chemistry, European Maastricht, pp. 567–568.
- Prinzhofer, A.A., Huc, A.Y., 1995. Genetic and post-genetic molecular and isotopic fractionations in natural gases. Chem. Geol. 126, 281–290. https://doi.org/ 10.1016/0009-2541(95)00123-9.
- Quan, Y.B., Hao, F., Liu, J.Z., et al.Wang, Z.F., 2017. Source rock deposition controlled by tectonic subsidence and climate in the western Pearl River Mouth Basin, China: evidence from organic and inorganic geochemistry. Mar. Petrol. Geol. 79, 1–17. https://doi.org/10.1016/j.marpetgeo.2016.10.028.
- Quan, Y.B., Liu, J.Z., Hao, F., et al., 2019. Geochemical characteristics and origins of natural gas in the Zhu III sub-basin, Pearl River Mouth Basin, China. Mar. Petrol. Geol. 101, 117–131. https://doi.org/10.1016/j.marpetgeo.2018.12.007.
- Sweeney, J.J., Burnham, A.K., 1990. Evaluation of a simple model of vitrinite reflectance based on chemical kinetics. AAPG Bulletin 10, 1559–1570. https://doi.org/10.1306/0C9B251F-1710-11D7-8645000102C1865D.
- Tang, Y., Jenden, P.D., 1998. Modeling gas isotopic fractionation during thermogenic gas generation. ABS-PAP-ACS 215 (Part 1), 3–GEOC.
- Tang, Y., Perry, J.K., Jenden, P.D., Schoell, M., 2000. Mathematical modeling of stable carbon isotope ratios in natural gases. Geochem. Cosmochim. Acta 64, 2673–2687. https://doi.org/10.1016/s0016-7037(00)00377-x.
- Tian, H., 2006. A study on the kinetic modeling of natural gas generation and gas accumualtion in the platform area of Tarim Basin. Guangzhou Institute of Geochemistry. Chinese Academy of Sciences, pp. 1–121. http://210.77.94.230: 8080/handle/344008/3524 (in Chinese).
- Tian, H., Xiao, X.M., Wilkins, R.W.T., et al., 2010. Genetic origins of marine gases in the Tazhong area of the Tarim basin, NW China: implications from the pyrolysis of marine kerogens and crude oil. Int. J. Coal Geol. 82, 17–26. https://doi.org/10.1016/J.COAL.2010.01.012.
- Tian, H., Xiao, X.M., Wilkins, R.W.T., et al., 2012. An experimental comparison of gas generation from three oil fractions: implications for the chemical and stable carbon isotopic signatures of oil cracking gas. Org. Geochem. 46, 96–112. https://doi.org/10.1016/j.orggeochem.2012.01.013.
- Tissot, B.P., Welte, D.H., 1984. Petroleum Formation and Occurrence, second ed. Berling-Verlag.
- Tissot, B.P., Pelet, R., Ungerer, P., 1987. Thermal history of sedimentary basins, maturation indices, and kinetics of oil and gas generation. AAPG (Am. Assoc. Pet. Geol.) Bull. 71, 1445–1466. https://doi.org/10.2310/6620.2008.08038.
- Ungerer, P., Pelet, R., 1987. Extrapolation of the kinetics of oil and gas formation from laboratory experiments to sedimentary basins. Nature 327, 52–54. https://doi.org/10.1038/327052a0.

- Wang, B.W., Xu, X.D., Wu, Y.Y., et al., 2020. Oil-gas origin and accumulation characteristics of Wenchang depression, western Pearl River Mouth Basin. Nat. Gas Geosci. 31, 980–992. https://doi.org/10.11764/j.issn.1672-1926.2020.01.008 (in Chinese).
- Wang, K., Y. J.R., Wu, J.F., Cao, Q., Liu, H., Tong, Z.G., 2014. Characteristics and evolution history of formation pressure in the Wenchang A Sag, Pearl River Mouth Basin. Geol. Sci. Technol. Inf. 33, 111–116+122 (in Chinese).
- Wang, K., Zhang, Y., Huang, S.B., Chen, J.Y., 2016. Characteristics and thermal evolution history of source rocks in the Wenchang A Sag, Pearl River Mouth Basin. Geol. Resour. 25, 196–203 (in Chinese). doi: CNKI:SUN:DZKQ.0.2014-04-018
- Wang, Z., Wang, Y., Wu, B., et al., 2017. Hydrocarbon gas generation from pyrolysis of extracts and residues of low maturity solid bitumens from the Sichuan Basin, China. Org. Geochem. 103, 51–62. https://doi.org/10.1016/j.orggeochem. 2016.10.011.
- Wang, Q., Zhang, D.Y., Wang, J., et al., 2018. Hydrocarbon and non-hydrocarbon charac-teristics for comprehensive identification about kerogen pyrolysis gas and oil cracked gas. Nat. Gas Geosci. 29 (9), 1231–1239 (in Chinese). doi: 10.11764/j.issn.1672-1926.2018.07.003.
- Waples, D.W., 2000. The kinetics of in-reservoir oil destruction and gas formation: constraints from experimental and empirical data, and from thermodynamics. Org. Geochem. 31, 553–575, https://doi.org/10.1016/S0146-6380(00)00023-1.
- Xia, X.Y., Chen, J., Braun, R., et al., 2013. Isotopic reversals with respect to maturity trends due to mixing of primary and secondary products in source rocks. Chem. Geol. 339, 205–212. https://doi.org/10.1016/j.chemgeo.2012.07.025.
  Xiao, X.M., Li, N.H., Gan, H.J., et al., 2009. Tracing of deeply-buried source rock: a
- Xiao, X.M., Li, N.H., Gan, H.J., et al., 2009. Tracing of deeply-buried source rock: a case study of the WC9-2 petroleum pool in the Pearl River Mouth Basin, South China Sea. Mar. Petrol. Geol. 26, 1365–1378. https://doi.org/10.1016/J.MARPFTGFO 2009 02 009
- Yang, J.H., Yang, X.B., You, J.J., et al., 2019. Hydrocarbon accumulation law and exploration direction in Zhu III depression, Pearl River Mouth Basin. Acta Pet. Sin. 40, 11–25. https://doi.org/10.7623/syxb2019S1002 (in Chinese).
- You, J.J., Liu, B., Hu, D.S., et al., 2024. Composition and distribution of lacustrine paleoproductivity during the deposition of hydrocarbon source rocks in Wenchang Sag, Pearl River Mouth Basin. Geol. Rev. 70 (2), 624–642. https://doi.org/10.16509/j.georeview.2023.10.031 (in Chinese).
- Zeng, L.F., 2020. Petroleum generation kinetics of jurassic Coaly source rocks in Junggar Basin. Guangzhou Institute of Geochemistry. Chinese Academy of Sciences, pp. 1–157. https://doi.org/10.27544/d.cnki.gzcds.2020.000014.
- Zhang, Y.Z., Xu, X.D., You, L., et al., 2014. Genesis of the natural gas in tight condensate gas reservoirs and forming model, Wenchang A Sag of Pearl River Mouth Basin. Nat. Gas Geosci. 25, 1320–1327. https://doi.org/10.11764/j.issn.1672-1926.2014.09.1320 (in Chinese).
- Zhang, S.C., He, K., Hu, G.Y., et al., 2018. Unique chemical and isotopic characteristics and origins of natural gases in the Paleozoic marine formations in the Sichuan Basin, SW China: isotope fractionation of deep and high mature carbonate reservoir gases. Mar. Petrol. Geol. 89 (Part 1), 68–82. https://doi.org/10.1016/j.marpetgeo.2017.02.010.
- Zhou, G., Zhang, Y.Z., Lu, J., et al., 2018. Reevaluation of high-quality source rock in the Wenchang Formation of the Wenchang B sag, the western Pearl River Mouth Basin. China Offshore Oil Gas 30, 28–37. https://doi.org/10.11935/j.issn.1673-1506.2018.03.004 (in Chinese).
- Zhu, W., Li, M., Wu, P., 1999. Petroleum systems of the Zhu III Sub-basin, Pearl River Mouth Basin, South China Sea. AAPG Bulletin 83, 990–1003. https://doi.org/10.1306/E4FD2E47-1732-11D7-8645000102C1865D.